Composites Part A 124 (2019) 105507

Contents lists available at ScienceDirect

Composites Part A

journal homepage: www.elsevier.com/locate/compositesa

Tensile properties of a stochastic prepreg platelet molded composite

Sergii G. Kravchenko*, Drew E. Sommer, Benjamin R. Denos, Anthony J. Favaloro, Clark M. Tow, William B. Avery, R. Byron Pipes

Composites Manufacturing & Simulation Center, Purdue University, 1105 Challenger Ave., West Lafayette, IN 47906, USA
Boeing Research and Technology, P.O. Box 3707, Seattle, WA 98124, USA

ARTICLE INFO

Keywords:
A. Molding compounds
B. Strength
C. Damage mechanics
C. Statistical properties/methods
Platelet

ABSTRACT

The stochastic prepreg platelet molded composite (PPMC) occurs when the orientation and arrangement disorder of platelets are determined by the uncontrolled molding conditions. The understanding of composite structure-property relationship is essential for the engineering applications of PPMCs. Computational analysis of the structure-property relationship in a PPMC with stochastic meso-scale morphology is herein performed under uniaxial tension conditions. The virtual distributions of tensile properties are obtained from the in-silico tensile tests based on the progressive failure analysis in the full-sized stochastically generated PPMC coupons. The developed analysis allows investigation of how the PPMC meso-structure details, such as platelet geometry and system morphology, define the variability in PPMC effective tensile properties.

1. Introduction

Prepreg platelet molded composite (PPMC) as a material form has been developed [1,2] to achieve a discontinuous composite system with controlled fiber length and 50–60% fiber volume fraction (FVF). PPMC starts as a continuous fiber (CF) prepreg tape, see Fig. 1(a), which is a material form that is well known and uniform in properties that can be either experimentally measured or micromechanically predicted. PPMC structures are fabricated by cutting and slitting the prepreg tape into platelets with a prescribed length, L_p, and width, w_p, then compression or transfer molding the platelets into the required geometries. The platelets inherit the initial fiber alignment, fiber volume fraction, and unprocessed thickness from the parent tape, but the discontinuities in the system allow for net shape molding processes. Having collimated fibers of the same length efficiently packed within a platelet, high fiber volume fraction is achieved in a PPMC. Owing to these characteristics, a PPMC provides for sufficient formability [3,4] and enhanced mechanical properties [5] as compared to the conventional discontinuous systems of dispersed “short”/”long” fibers [6] for compression molding, such as sheet molding compounds (SMC) and bulk molding compounds (BMC) with FVF in the range 10–30%. Furthermore, molding with prepreg platelets opens wide opportunities for the trim- scrap reutilization [7,8], which has a significant role in reducing the cost and environmental impact of composites manufacturing. PPMCs are currently in production for use in aircraft and automobile structures; nevertheless, the current level of understanding of PPMC requires a substantial amount of experimental proof testing of the finished parts, which can be reduced by the development of the fundamental knowledge of the origins of composite properties from underlying composite structure (i.e. the composite structure–property relationship).

Macroscale is the largest length scale where the overall mechanical performance under some loading conditions is evaluated. As pointed out by Lakes [9], a structure may be present on several scales in the material, but the largest structural element scale typically controls the effective (macroscopic) response of the material system. A PPMC system has two easily recognized scales of heterogeneity where structure can be seen, namely a micro-scale where individual fibers are distinguishable, and a meso-scale, meaning the scale where individual platelets are distinguishable. The fibers and matrix are the micro-constituents of the PPMC as they are building blocks of a platelet, while the platelets are the building blocks in a PPMC at the meso-scale. A PPMC has the major stress concentrations in the meso-scale stemming from the discontinuities between individual platelets. The local meso-scale interactions between platelets determine the dominant factors that control the progressive damage and macroscopic failure strength of a PPMC, i.e. the meso-scale stress transfer defines the macroscopic response of the composite. The meso-scale stress transfer between interacting platelets depends on the details of composite *meso-structure*. Therefore, a PPMC derives its effective mechanical properties from the complex meso-scale structure. The *meso-scale structure* of a PPMC is defined by the *platelet geometrical parameters* and *meso-scale morphology*, which is characterized by the arrangement (overlapping), orientation

* Corresponding author at: Composites Manufacturing & Simulation Center, Purdue University, 1105 Challenger Ave., West Lafayette, IN 47906, USA.
E-mail address: skravche@purdue.edu (S.G. Kravchenko).

https://doi.org/10.1016/j.compositesa.2019.105507
Received 2 April 2019; Received in revised form 18 June 2019; Accepted 29 June 2019
Available online 02 July 2019
1359-835X/

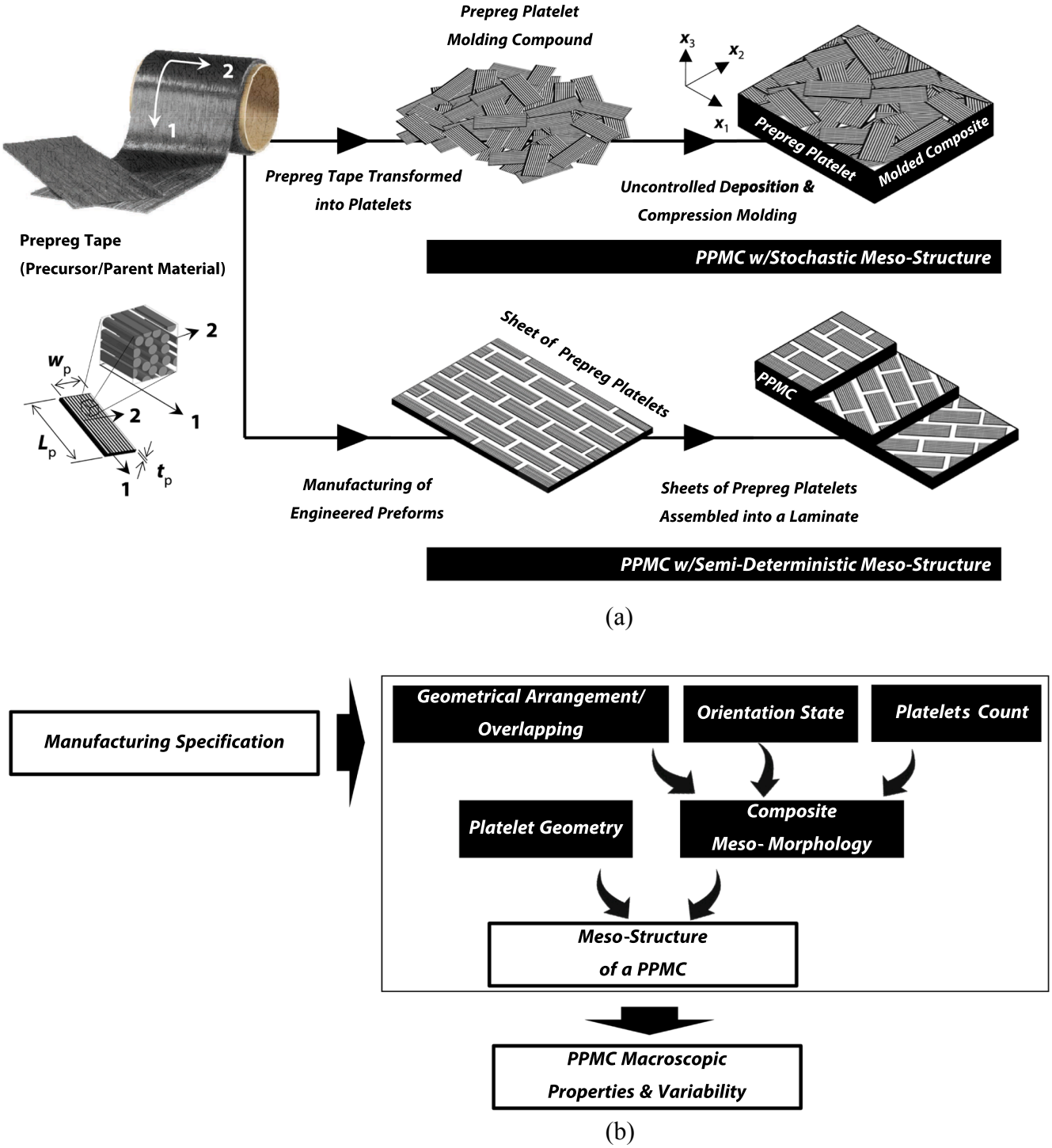

Fig. 1. (a) Morphological forms of a prepreg platelet molded composite (PPMC) system; (b) Process-structure-property relationship in a PPMC along with the definition of the PPMC meso-structure descriptors. (For interpretation of the references to colour in this figure legend, the reader is referred to the web version of this article.)

and number of platelets in the system, as schematically summarized in Fig. 1(b).

Prepreg platelets may be processed into different forms resulting in the PPMC systems of varying morphological complexities, as schematically summarized in Fig. 1(a). For example, a *semi-controlled morphology* with a *deterministic* orientation state can be engineered by introducing the regular pattern of cross-fiber cuts into the CF prepreg plies to produce sheets of aligned and staggered platelets [10,11]; thereafter, these preforms (sheets) are assembled at different angles to fabricate a multidirectional laminate with a desired orientation state. Although in practice the overlap distribution between platelets from adjacent plies is obtained in a non-controlled way and is essentially non-deterministic, the resulting PPMC meso-structure can be classified as semi-deterministic due to the controlled orientation state. Alternatively, a *stochastic meso-structure* of a PPMC is achieved when the orientation and arrangement disorder of platelets result from their uncontrolled initial positioning in the mold and further anisotropic flow of heterogeneous compound, causing relocation and reorientation of

platelets, while the molding process results in the non-deterministic local geometrical dimensions (thickness and width) of processed platelets. Thereafter, platelets are structurally arranged at various angles relative to one another to produce irregular semi-laminated morphology, where the majority of platelets are planar-distributed although platelets may bend around their neighbors to form wavy compliant overlaps. Stochastic local structural arrangement and orientations of platelets along with non-constant platelet dimensions vary throughout the volume of a PPMC and have a major role in the failure mechanisms since damage in the composite seeks out the locations where a local meso-scale stress concentrations yield the possible failure sites.

Stochastic manufacturing process incorporates uncertainty into PPMC meso-structure, which translates into the largely scattered effective stiffness and strength measured in typical size tensile coupons [12]. The scaling and variability of effective mechanical properties strongly depend on the stochastic PPMC meso-structure descriptors as different research groups have reported [5,8,13–17]. The previous experimental characterization of stochastic PPMCs showed that: (*i*) the composite tensile properties increased with platelet length (for constant platelet thickness), while longer platelets provided for increased variability of properties [18,5,14]; (*ii*) the thinner parent tape provided for reduced variability and increased averages of properties [15,19]; (*iii*) increased coupon thickness improved the properties [5].

An ability to design the desired combinations of properties a PPMC comes with increased understanding of the origins of macroscopic properties from the composite meso-structure determined by the manufacturing specification [20]. The study of the *structure-properties relationship* is fundamental for the development of a PPMC compatible with intended application. *Computational analysis* of the structure-property relationship, which is the main motivation of the present work, allows to virtually investigate the design space of control parameters of PPMC meso-structure. Virtual material design is a valuable tool, since it aids in addressing the effects of material variables prior to the manufacturing and, thus, reducing the trial-and-error efforts in material development for tailored properties [21,22]. In this work, the authors will show that all descriptors of the meso-structure are responsible for scaling and variability of the PPMC macroscopic properties.

The analysis methods for unidirectional short fiber composites (SFC) and multidirectional SFC (modified rule of mixtures, laminate analogy) are not appropriate for the analysis of a PPMC, as they (*i*) do not have fibers as building blocks at the meso-scale and (*ii*) generally speaking, disregard the morphological complexity of a composite. A number of computational meso-scale models to evaluate the effective properties of stochastic PPMC tensile coupons were recently proposed [23–28]. The analysis methods that oversimplify or neglect the realistic morphology details of a composite, though useful for certain applications, have intrinsic limitations on predictive capabilities of composite properties stemming from inability to describe the internal stress distributions in composite elements. Given the spatial complexity of a PPMC stochastic meso-structure, a computational model amenable for the analysis of structure-property relationship is expected to account for the three-dimensional meso-structure dependent stress transfer.

The main objective of this work is to develop a computational analysis to *simulate and explain the scaling and variability* of effective tensile properties (stiffness and strength) of a stochastic PPMC from the known deterministic properties of a platelet parent material and stemming from the details of composite meso-structure. The focus is to investigate by simulation (in-silico) different size effects associated with the variable meso-morphology and modified geometrical characteristics such as: (*i*) the influence of the platelet dimensions, (*ii*) the effect of tensile coupon thickness, and (*iii*) the effect of the orientation state in a coupon on probabilistic values of stochastic PPMC stiffness and strength. The analysis of probabilistic distribution of stochastic PPMC tensile properties has its foundation in the progressive failure analysis (PFA) of virtual (digital) full-sized tensile coupons with modified descriptors of explicitly modeled meso-structure, meaning that PFA is conducted for repeated random sampling of virtual meso-morphologies. The PFA is performed within the framework of continuum damage mechanics wherein a platelet is considered a damageable homogeneous orthotropic material having the mechanical constants of the parent prepreg tape. The Monte-Carlo (probabilistic) approach to virtual testing enables quantification of the variation and uncertainty of stochastic PPMC tensile properties caused by the variability of meso-structure by obtaining the distributions of properties instead of fixed values, where a distribution describes the range of possible values and shows which values within the range are most likely. Basic methods of statistics are used (*i*) to validate the results of probabilistic modeling against the experimental data and (*ii*) to compare the property distributions for the modified control parameters of the virtual meso-structure samples. The proposed analysis is shown to support the experimental observations and, therefore, is useful for the virtual study of the structure-property relationship in a PPMC.

2. Experimental work

2.1. Manufacturing of stochastic PPMC tensile coupons with various orientation states and thicknesses

Several groups of coupons were manufactured to study (*i*) the effect of coupon thickness and (*ii*) the effect of platelets alignment on the distribution of effective tensile properties of a stochastic PPMC. The test matrix is summarized in Table 1. Platelets with $L_p \times w_p = 12.7 \times 12.7$ mm were obtained from a unidirectional carbon fiber/thermoplastic prepreg tape AS4/PEKK supplied by Cytec/Solvay. Selected coupons from different batches were CT-scanned and the average degree of platelet fiber alignment, a_{11}, with the loading direction (x_1) was analyzed with VGStudio MAX using the methodology explained in [29] and reported in Table 1.

Stochastic orientation state of the meso-morphology depends on the manufacturing conditions during the molding process. A “low- flow” process [30] is typically referred to as molding with minimal change of platelet orientation during compaction. It stems from the full mold coverage with a charge (compound) of platelets under no control of their arrangement. A square flat mold was herein used to manufacture the “low-flow” plaques with planar dimensions of 254 × 254 mm (10 × 10in). The charge of platelets was deposited into the mold, then heated to 380 °C to reach the melt temperature of the polymer, and subsequently pressed at 6.9 MPa (1000 psi). The tool was then air-cooled and the plaque was demolded. Structural adhesive was used to bond the 50.8 mm (2 in)- long fiber-glass tabbing strips to either end of the molded plaque. Individual tensile coupons were then cut from a tabbed plaque. Ten-inch long coupons had a final gage length, *L*, of 152.4 mm (6in) and width, *w*, of 25.4 mm (1in).

Flow conditions can modify the stochastic orientation state in a PPMC. The “flow-aligned” and “high-flow” coupons were manufactured to have a preferential alignment of platelets induced by the flow conditions. In the first approach, a flat plate was compression molded from a center charge (40% charge coverage) in squeeze flow to extract the so-called “flow-aligned” coupons. The details of manufacturing of “flow-aligned” tensile coupons can be found in [31]. Elongation of the charge during molding caused the preferential alignment of platelets in the direction of flow, coincident with subsequent loading direction. The flow induced orientation state remains stochastic by nature but possesses a higher degree of global alignment (a_{11}). In the second approach, the charge of platelets was placed in the charge cavity and forced to flow into the horizontal channels through the vertical sprue producing the so-called “high-flow” coupons.

2.2. DIC complemented tensile testing of PPMC coupons

The effective elastic and strength properties of stochastic PPMC

Table 1
Test matrix.

Platelet size, $L_p \times w_p$	Type of stochastic orientation state	Sample size	Avg. coupon thickness, t	Manufacturing method	CT-measured coupon-level a_{11}	
					No. of coupons	Avg.
12.7 × 12.7 mm	"Low-flow"	10	0.8 mm	Full mold coverage with platelet charge	N/A	N/A
		13	1.4 mm		N/A	N/A
		20	3.7 mm		5	0.535
		24	7 mm		5	0.594
	"Flow-aligned"	8	3.92 mm	40% mold coverage with a charge made of stacked plaques previously obtained by pressing the platelets in a fully covered mold	3	0.707
	"High-flow"	3	3.84 mm	Platelet charge experienced plug flow in a transfer molding process	3	0.633

coupons were measured in the uniaxial displacement-control tension test. The coupons were coated with white spray paint and a random pattern of black speckle marks was applied for Digital Image Correlation (DIC) to measure the strains. Tensile tests were performed in a 22-kip-MTS material testing system with crosshead rate of 2 mm/min. Coupons were loaded in the test frame and 5-megapixel DIC images from two cameras were captured with Correlated Solutions' VIC-SNAP software. DIC-measured displacements were used to calculate full field Green-Lagrangian strain distribution during loading history. The average Lagrangian strains in the loading x_1-direction, $\bar{\epsilon}_{11}$ (Ω), determined by the DIC analysis on the front face of a coupon were plotted against effective tensile stress, $\bar{\sigma}_{11}$, to characterize the macroscopic response of a PPMC coupon [5,16]. Global strain, $\bar{\epsilon}_{11}$ (Ω), was calculated over the entire speckled surface of the coupon,Ω , 127 × 25.4 mm (5 × 1in) as shown in Fig. 2. Effective stress was calculated from the force channel in the test machine as force divided by the coupon average cross sectional area ($w \times t$). Example stress-strain curves are shown in Fig. 3. Effective tensile modulus of a coupon was evaluated as the slope of the $\bar{\sigma}_{11}$-$\bar{\epsilon}_{11}$ curve over the strain interval of 100 to 2000με. The ultimate strength of a coupon is recorded as an abrupt load drop when a critical state of damage is reached for a macroscopic crack to be formed to separate a coupon into two pieces.

The initial linear global response of a coupon is followed by the progressive global stiffness degradation leading to a non-linear macroscopic stress-strain ($\bar{\sigma}_{11}$-$\bar{\epsilon}_{11}$) relation before the ultimate strength is reached, see Fig. 3. The evolution of local damage within a coupon reflected in the non-linear portion of the global stress-strain curve is recognized by the multiple audible crack events (distinct clicking sounds, "pings" and "tings" also previously reported in [32]). The meso-scale heterogeneous composite system of many platelets is a highly redundant structural system. This means that a PPMC is able to form multiple simultaneous precursory damage sites and develop alternative paths for damage progression during a typical tensile test. Therefore, a prominent feature of a PPMC is the coexistence of the primary and several secondary failure sites during loading, which can be observed in a coupon post-mortem. Local meso-scale cracks form early in the loading history of a coupon and progressively develop until one of them grows into the macroscopic crack running from one edge of the coupon to another and providing for the major/primary failure site, while the rest of the cracks can be termed as secondary failure sites. The observation of post-mortem coupons indicates that the complex topology of the macro-crack is defined by the details of coupons local meso-morphology. The number and extent (or size) of secondary failure sites, i.e. the damaged regions competed for but not resolved into formation of the macro-crack, depend on the details of the PPMC meso-structure. Fig. 2 shows one example of the two large-scale developing cracks visible with a naked eye before ultimate strength is reached, and eventually one of them matures into a macroscopic crack while the other one remains a secondary damage. Fig. 4 shows an example wherein the internal damage distribution was inspected. Therein, the major failure site, a macro-crack, has been developed in the upper portion of the coupon, while there was a substantial internal damage in the lower portion made visible via the CT-scanning of a post-mortem coupon. Internal damage also appeared as a series of edge cracks well seen through optical microscopy.

2.3. Statistical significance methods

Since the mechanical properties of a stochastic PPMC exhibit largely scattered distributions, the statistical analysis is a necessary tool to understand the effects of meso-structure control parameters on the composite properties. In the following work, the batches of PPMC coupons with modified characteristics of stochastic meso-structure are tested (experimentally and virtually) to study if the distributions of effective tensile stiffness and strength significantly depend on the varied meso-structure characteristics. The collection of measurements

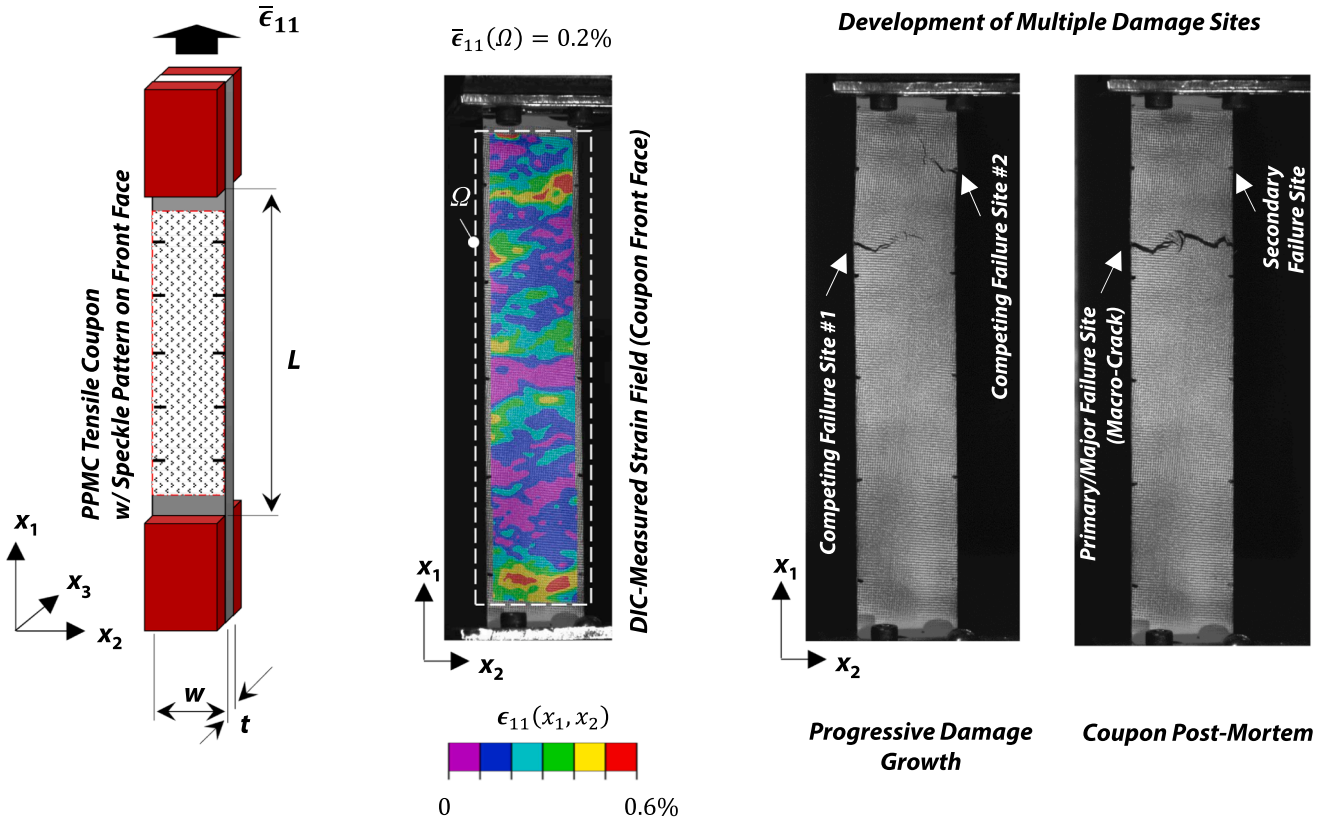

Fig. 2. Tensile coupon schematic (left) and DIC-analyzed strain field along with photographs of the damage topology (at two loading instances) from the front face of a selected PPMC coupon (right). (For interpretation of the references to colour in this figure legend, the reader is referred to the web version of this article.)

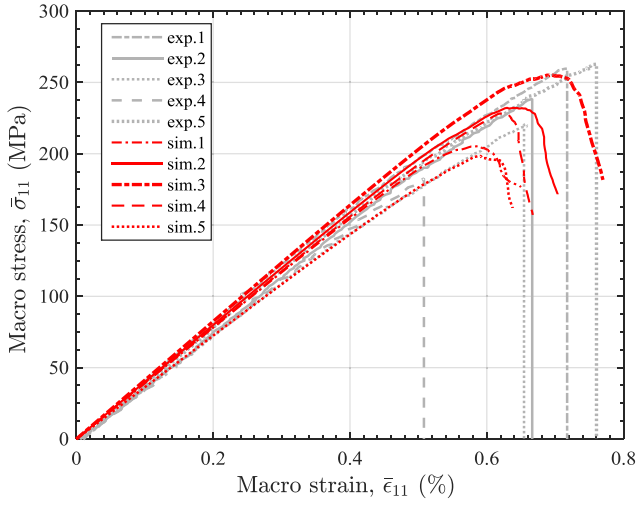

Fig. 3. Effective tensile response of stochastic PPMC coupons: experimental ("exp") and simulation ("sim") results. Average thickness, *t*, of experimental coupons is 3.7 mm; thickness of in-silico coupons is 3.5 mm. Platelet dimensions in the simulation are $L_p \times w_p \times t_p = 12.7 \times 12.7 \times 0.14$ mm. (For interpretation of the references to colour in this figure legend, the reader is referred to the web version of this article.)

taken from a population of a specified batch of coupons represents a data sample. The Anderson-Darling (A-D) test for normality is used to detect the departure from normality of the data samples. To ensure the existence of a relationship between the PPMC tensile properties and a modified meso-structure characteristic, statistical significance of the observed difference between the samples is analyzed by the two-sample Welch's *t*-test and two-sample Kolmogorov- Smirnov (K-S) test [33] to compare the averages and cumulative distribution functions (CDFs), respectively. The two-sample tests determine if the hypothesis of the two samples representing the same distribution can be rejected or not at the certain significance level (SL). The difference between the data samples is herein deemed statistically significant if the probability of the phenomenon being random is less than 5%, resulting in the *p*-value less than 0.05.

2.4. Scaling of stochastic PPMC tensile stiffness and strength by coupon thickness (Experimental)

Herein we experimentally invesitigate the research hypothesis if the distributions of tensile stiffness and strength are dependent on the thickness of PPMC coupons with stochastic meso-structure. Four batches of PPMC coupons (with a platelet size $L_p x w_p = 12.7 \times 12.7$ mm) were made with average thickness of 0.82 mm (cov. 5.7%), 1.4 mm (cov. 5.3%), 3.73 mm (cov. 0.8%), and 6.9 mm (cov. 7.9%). Table 2 gives the number of coupons within each batch (sample size). The distribution of tensile modulus and strength data is shown in Fig. 5. The samples were quantitatively screened by the maximum normal residual method for the outliers. The two-sample tests were used to analyze the means and CDFs from the smallest to the largest coupon thickness to determine which distributions are and are not significantly different with corresponding *p*-values reported in Table 2. Effective stiffness and strength of a stochastic PPMC seem to scale substantially with material thickness. It follows that the overall coupon average stiffness improves from about 30 GPa to 40 Gpa when coupon thickness is increased from less than 1 mm to about 3.7 mm, while the average effective strength showed two-fold increase going from the thinnest to the thickest coupons, being doubled from about 100 MPa to over 200 MPa. Statistical analysis showed that both mean values and cumulative distributions of stiffness and strength of 0.82 mm, 1.43 mm, and 3.7 mm thick coupons are significantly different at the 5% significance level (*p*-values < 0.05), while the null hypothesis cannot be rejected (with 95% confidence

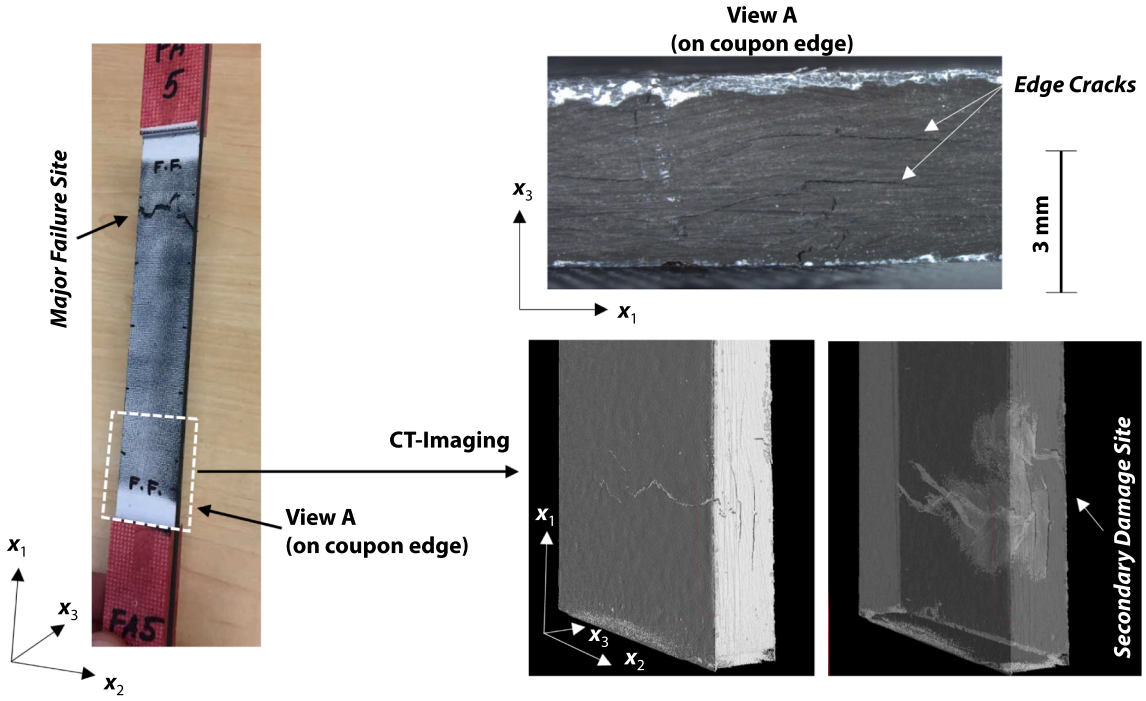

Fig. 4. Internal secondary damage observed with CT-imaging, edge cracks and a major failure site (macro-crack) in a selected coupon. (For interpretation of the references to colour in this figure legend, the reader is referred to the web version of this article.)

level) for the samples of 3.7 mm and 7 mm thickness (p-value > 0.05).

3. In-Silico uniaxial tensile test of a stochastic PPMC

This section describes the development, application and interpretation of results of a computational finite-element (FE) model to predict macroscopic stiffness and strength of a stochastic PPMC by the simulation of a uniaxial tensile test of a full-sized virtual coupon with semi-laminated stochastic meso-scale morphology and deterministic platelet size.

The three-dimensional meso-morphology of a stochastic PPMC is explicitly modeled for the analysis of meso-structure dependent effective tensile properties of the composite. The utilized meso-scale computational approach considers individual platelets as transversely isotropic homogenized material with properties of the prepreg tape. The PFA at the local platelet level is based on the (*i*) stiffness reduction scheme and (*ii*) smeared crack approach realized for the constitutive tensor of the platelet material, and consists of computing the platelet-level stresses and strains, which are then used as input to the selected failure model. The overall (macroscopic, or effective) behavior of a PPMC coupon is defined by the interactions between individual platelets.

The meso-scale morphological details of a PPMC coupon are explicitly incorporated into the computational model to ensure an adequate three-dimensional meso-scale stress analysis, as the scale of a single platelet is not separable from the scale of a laboratory tensile coupon for the platelet sizes used in practice. Some realistic morphological features such as complex platelets arrangement and variable platelet orientation are reflected in a virtual material architecture to obtain the reliable prediction of mechanical properties. A "computational window" size of a PPMC meso-structure sample for virtual (in-silico) testing is selected to have the typical dimensions of a full-sized tensile coupon, as there are no smaller volumes representative of the full coupon meso-structure amenable for the computational analysis of composite properties to compare them to the experimental data at the macroscopic level of observation.

Progressive local meso-scale damage in a platelet is mathematically expressed as a permanent weakening (i.e. loss of stress carrying capacity) at material points by means of continuum damage mechanics (CDM), which treats the effects of PPMC "meso-cracks" by locally reducing ("softening") the corresponding components of the platelet constitutive tensor [34]. CDM allows prediction of both initiation and propagation of damage without making a modification to the original FE mesh of the structural system, i.e. without geometrically modeling such cracks by the insertion of discontinuities into the original FE mesh. Thus, in a smeared crack approach, the nucleation of one or more "cracks" in the volume that is attributed to an integration point is translated into a deterioration of the current stiffness and strength at

Table 2
Statistical analysis of variation of PPMC tensile properties with coupon thickness, obtained experimentally.

Coupon avg. thickness (mm)	Sample size	Tensile stiffness (Experimental)						Tensile strength (Experimental)					
		Avg. (GPa)	St. Dev. (GPa)	COV(%)	p-value			Avg. (MPa)	St. Dev. (MPa)	COV (%)	p-value		
					A-D test	t-test	K-S test				A-D test	t-test	K-S test
0.8	10	29.53	2.83	9.60	0.31			112.33	12.62	11.24	0.102		
1.4	13	33.70	2.59	7.69	0.02	$1.8\ (10^{-3})$	$6.1\ (10^{-3})$	167.83	29.57	17.62	0.206	$1.2\ (10^{-5})$	$5.6\ (10^{-5})$
3.7	20	39.92	2.26	5.66	0.81	$3.0\ (10^{-7})$	$2.5\ (10^{-7})$	218.07	31.76	14.56	0.292	$8.1\ (10^{-5})$	$1.2\ (10^{-3})$
7	24	39.23	3.83	9.76	0.63	0.485	0.58	228.76	27.72	12.12	0.657	0.246	0.53

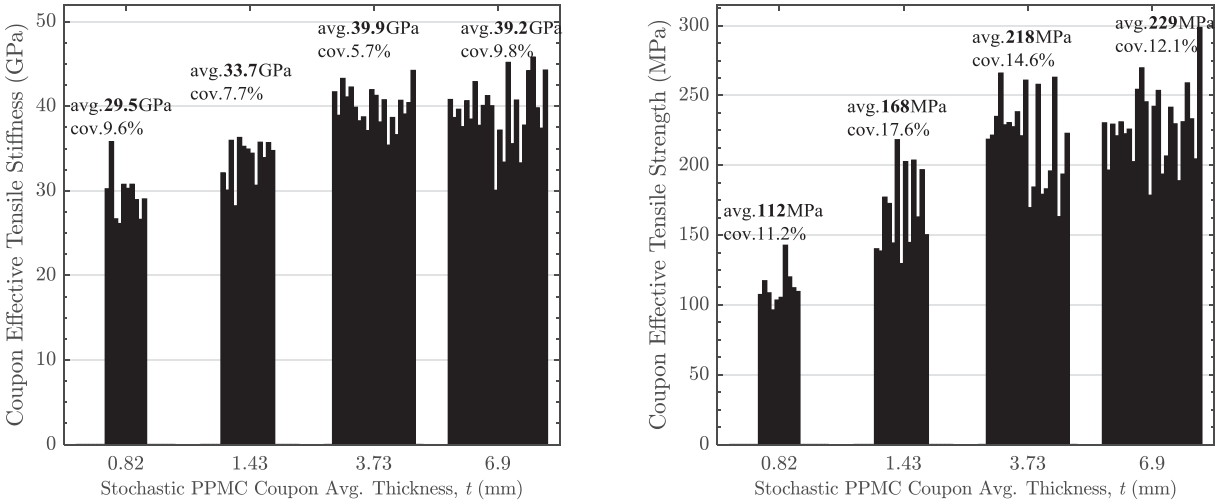

Fig. 5. Experimental tensile stiffness and strength of a stochastic PPMC made with 12.7 × 12.7 mm platelets as a function of coupon thickness.

that integration point via scalar damage variables, allowing multiple assumed meso-scale damage mechanisms to interact.

3.1. Assumptions for analysis

Platelet volume fraction in a tensile coupon is assumed 100%, although in reality a physical coupon may have up to 10% of neat resin pockets [18]. Local platelet thickness and width variation in a physical PPMC is not addressed in the simulation, meaning the platelet dimensions are considered constant in a given virtual coupon. Homogenized properties of the prepreg tape (parent platelet material) are assumed deterministic, meaning that the local fiber volume fraction variability in a platelet and the dependence of in-situ lamina strength on CF UD ply thickness are not considered.

3.2. Computational model for virtual tension test of a PPMC coupon with deterministic platelet size and stochastic meso-scale morphology

The multi-directional stochastic PPMC is *approximated* as a continuum in the $(x_1x_2x_3)$ space with sub-domains assigned local coordinate systems $(1_i2_i3_i)$ to represent stacked misaligned platelets. Fig. 6 shows an example of the domain occupied by a virtual stochastic PPMC coupon as a collection of sub-domains representing the misaligned individual platelets (shown in different colors) with defined boundaries, which create local stiffness discontinuities that control meso-scale interactions between platelets and, therefore, their collective mechanical response.

The meso-structures of virtual coupons are constructed in DIGIMAT FE [35] with the sequential adsorption algorithm. It means that stochastic structural arrangement and orientation of platelets is *approximated* by the random placement algorithm, where platelets are placed sequentially by generating their center points and angles according to the probability distribution functions (PDFs) by means of a pseudo-random number generator. The sampling of pseudo-random numbers is from the uniform probability distribution function for platelet centroids, while the orientation probability distribution is extracted from the requested second- order orientation tensor (OT) [36], $\boldsymbol{a}_{ij}$, which is a convenient large-scale descriptor of the orientation distribution in a composite system containing a large number of misaligned platelets. The discrete form of the OT for N platelet fiber orientation vectors, $\{\boldsymbol{p}^{(k)}\}_{k=1}^{N}$, is given by Eq. (1):

$$\boldsymbol{a}_{ij}^{\{\boldsymbol{p}^{(k)}\}_{k=1}^{N}} = \frac{1}{N}\sum_{k=1}^{N}\begin{bmatrix} (p_1p_1)_k & (p_1p_2)_k & (p_1p_3)_k \\ \cdots & (p_2p_2)_k & (p_2p_3)_k \\ sym & \cdots & (p_3p_3)_k \end{bmatrix} \quad (1)$$

where $\boldsymbol{p}^{(k)} = \{p_1 \;\; p_2 \;\; p_3\} = \{\cos\theta\sin\varphi \;\; \sin\theta\sin\varphi \;\; \cos\varphi\}$ is a vector of the k^{th} platelet fiber direction ("1"), which orientation in the global coordinate system $(x_1x_2x_3)$ is defined as shown in Fig. 6. Local 12-plane of a platelet and the global x_1x_2-plane are coplanar when the a_{33} term is requested zero ($\varphi = 90^\circ$). The recovery of the orientation distribution function (ODF) from the requested a_{ij} is achieved by using the fourth-order orientation tensor $\boldsymbol{a}_{ijkl}$, which is constructed by the fitted orthotropic closure approximation [37]. The "2D-random" is a special case of the second-order OT, $\boldsymbol{a}_{ij}$ = [[0.5,i 0, 0] [0, 0.5, 0] [0, 0, 0]], equivalent to sampling random numbers from the uniform ODF.

Meso-structure geometry and mesh generation are combined in a voxel-based process. The coupon volume is discretized with a regular grid (pattern) of three-dimensional units, voxels, of selected size. This grid is known as a voxel mesh. Then, platelets with defined size and orientation are sequentially placed within the voxel mesh. All voxels that lie within the platelet's boundaries are identified as those belonging to this platelet. Hence, all platelets consist of collections of voxels, and any voxel within the coupon volume belongs to only a single platelet. The packing of virtual platelets is essentially the packing of clusters of mutually orthogonal parallelepipeds inside a given domain (which is a "coupon"). When a new platelet is laid above another (already existing) platelet, the unsupported segment of a new platelet will "sink" down while the overlapping part will remain on top of the existing platelet, which creates curved platelets. Thus, the full three-dimensional character of a PPMC is preserved in a digital tensile coupon since the virtual platelet placement proceeds throughout the thickness of the tensile coupon, allowing for multiple and complex-structured overlaps of platelets. For positions near the edges of the coupon domain, it is possible for the platelet to extend beyond the boundaries of the domain, meaning a platelet may have a portion lying outside of the domain occupied by the coupon. Allowing the platelets to extend beyond the boundaries of the coupon domain simulates the random sectioning of a coupon volume from a larger volume (like a plaque), where some platelets will inevitably intersect the surface of a coupon domain. The voxelized morphology is output as a FE mesh for subsequent PFA, where each voxel becomes an eight-node brick FE. All platelet elements are assigned the same homogenized material properties of prepreg tape, and the local orientation is mapped from geometry to the FEs. Neighboring elements with similar local material orientation thus represent a single platelet. Fig. 6 shows two voxelized platelets (i, j) along with their local material coordinate systems $(1_i2_i, 1_j2_j)$, where "*1*" is the local platelet fiber direction and "*2*" is the local transverse direction. Single parallelepiped FE (voxel) thickness is herein a required platelet thickness, while its length and width were taken 0.7 mm. The main idea behind the voxel based representation is to avoid conformal meshing of

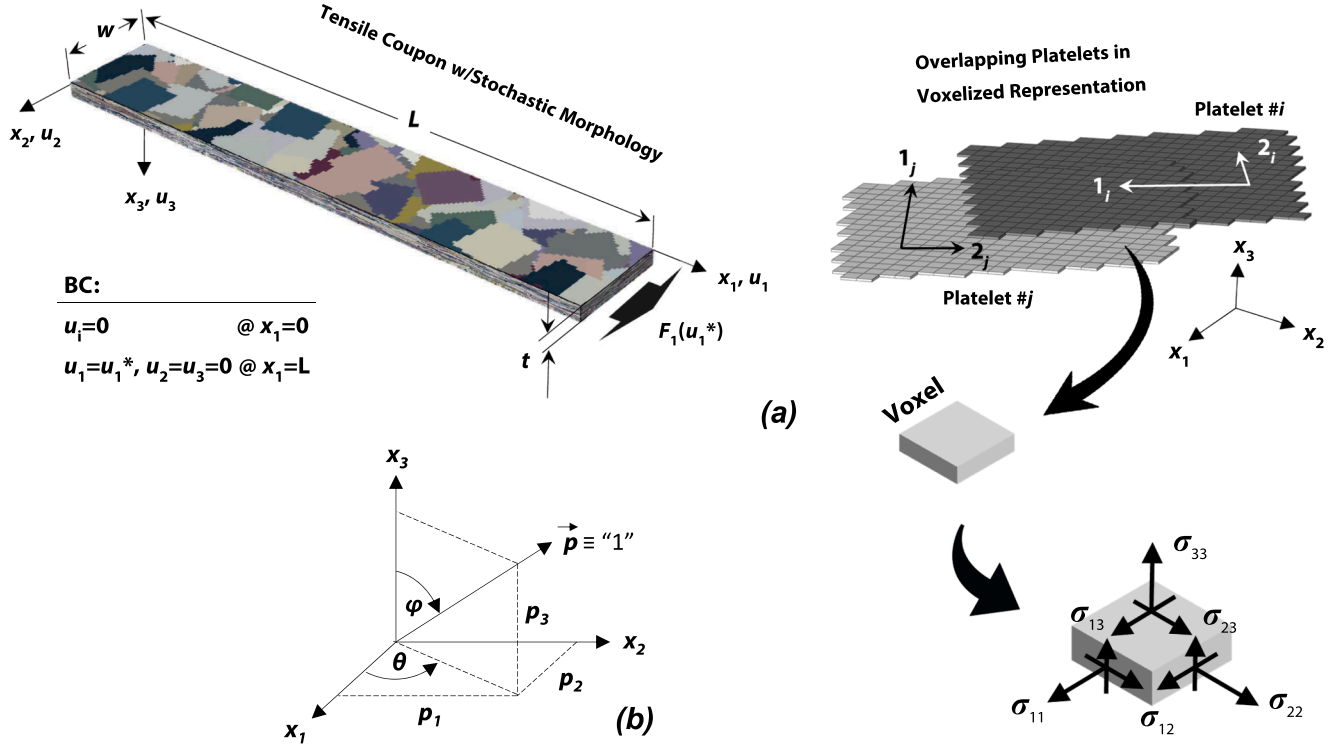

Fig. 6. (a) Voxel-based finite element model of a virtual tensile coupon with prepreg platelet meso-structure; (b) Platelet fiber direction vector in the global coordinate system. (For interpretation of the references to colour in this figure legend, the reader is referred to the web version of this article.)

exact platelet shapes. The voxel-based meshing technique is the simplest to implement providing for the very high mesh quality as the voxels (brick elements) have good quality metrics [38]. The drawback of the voxel-based mesh is in producing the surface structures that are aliased or "stair-stepped".

The virtual coupon global length, width and thickness are labeled as L, w and t, respectively. The boundary conditions on a virtual coupon are as follows: one edge ($x_1 = 0$) is fixed while the opposite edge ($x_1 = L$) is uniformly pulled along the x_1-direction with displacement u_1^* and clamped against other displacements, as schematically illustrated in Fig. 6. The non-linear quasi-static finite element analysis (FEA) is carried out with a commercial FE code ABAQUS/Standard (Implicit) 6.14-1. The platelets are modeled with solid three-dimensional stress elements (C3D8).

A non-linear quasi-static problem is unstable because of the progressive local material softening. To help convergence behavior in an implicit solution procedure of ABAQUS/Standard [39], the automatic stabilization is used through the addition of volume-proportional damping to the model. The damping factor, a fraction of the allowed dissipated energy to the strain energy, is set to 1 (10^{-4}). Furthermore, the non-default solution control parameters for ABAQUS [39] convergence control algorithm and the load (pseudo-time) incrementation were found useful in improving the solution efficiency. By using a "discontinuous analysis", the default load incrementation parameters I_0 and I_R [39] were changed to 8 and 10, respectively. The default value of I_A, the maximum number of cutbacks allowed for an increment, was increased from 5 to 20.

3.3. Three-dimensional meso-scale constitutive model for damageable platelet material

The assumed primary local meso-scale failures that develop within a PPMC include platelet in-plane and out-of-plane damage. Platelet in-plane damage modes imply the loss of ability to support the in-plane stresses (σ_{11}, σ_{22}, σ_{12}), representing the platelet transverse damage (platelet splitting along the fibers) and platelet fracture across the fibers. Out-of-plane platelet damage implies the loss of integrity in the coupon through-thickness direction (delamination between platelets), when interlaminar stresses (σ_{33}, σ_{23}, σ_{13}) can no longer be transmitted from one platelet to another. As a physical crack implies the stress transfer disruption, a local cracked region can be modeled as a region with degraded stiffness. Stiffness discount/degradation with internal damage variables is a typical approach to computationally represent damage development [40]. The progression of the local meso-scale platelet damage modes is treated in the simulation with elastic-brittle CDM, wherein the meso-scale damage variables are introduced to modify the platelet *stress-strain constitutive tensor* (without displacement discontinuities) based on the damage onset and propagation criteria.

The platelet constitutive model herein utilized is modified from Linde et al. [41] and employed as a user material (UMAT) FORTRAN subroutine [39] for ABAQUS /Standard (Implicit). The platelet is considered as an orthotropic homogenized continuum in which in-plane and out-of-plane damage is the result of the tri-axial state of stress as given by Eq. (2):

$$\begin{Bmatrix} \sigma_{11} \\ \sigma_{22} \\ \sigma_{33} \\ \sigma_{12} \\ \sigma_{13} \\ \sigma_{23} \end{Bmatrix} = \boldsymbol{C_d} \left\{ \begin{Bmatrix} \epsilon_{11} \\ \epsilon_{22} \\ \epsilon_{33} \\ 2\,\epsilon_{12} \\ 2\,\epsilon_{13} \\ 2\,\epsilon_{23} \end{Bmatrix} - \Delta T \begin{Bmatrix} \alpha_{11} \\ \alpha_{22} \\ \alpha_{33} \\ 0 \\ 0 \\ 0 \end{Bmatrix} \right\} \tag{2}$$

where $\boldsymbol{C}(\boldsymbol{d})$ is the damaged stiffness matrix given in Eq. (3); ΔT is the temperature differential; α_{ij} are the coefficients of thermal expansion. The damaged stiffness matrix depends on the virgin (undamaged) stiffness components of prepreg tape and three damage variables, with d_1, d_2 and d_3 reflecting the state of damage in the fiber, transverse to the fiber and out-of-plane directions of a platelet, respectively. The virgin stiffness components, C^0_{ij}, are expressed in terms of elastic moduli of the platelet's parent unidirectional continuous fiber tape.

$$\boldsymbol{C}(\boldsymbol{d}) = \begin{bmatrix} (1-d_1)C_{11}^0 & (1-d_1)(1-d_2)C_{12}^0 & (1-d_1)C_{13}^0 & 0 & 0 & 0 \\ & (1-d_2)C_{22}^0 & (1-d_2)(1-d_3)C_{23}^0 & 0 & 0 & 0 \\ & & (1-d_3)C_{33}^0 & 0 & 0 & 0 \\ & symm & & (1-d_1)(1-d_2)C_{44}^0 & 0 & 0 \\ & & & & (1-d_3)C_{55}^0 & 0 \\ & & & & & (1-d_3)C_{66}^0 \end{bmatrix}, \tag{3}$$

Table 3
Material constants for platelet constitutive tensor.

Material property	Numerical value
Longitudinal modulus, E_{11} [GPa]	130.7
Transverse modulus, E_{22} (E_{33}) [GPa]	9.6
Shear modulus, G_{12} (G_{13}) [GPa]	5.7
Shear modulus, G_{23} [GPa]	4.0
Poisson's ratios, ν_{12} (ν_{13})	0.32
Poisson's ratio, ν_{23}	0.4
Longitudinal coefficient of thermal expansion, α_{11} [$\mu\epsilon/^0$C]	1
Transverse coefficient of thermal expansion, α_{22} (α_{33}) [$\mu\epsilon/^0$C]	25
Longitudinal tensile strength, X_t [MPa]	2157
Longitudinal compressive strength, X_c [MPa]	1270
Transverse tensile strength, Y_t [MPa]	78
Transverse compressive strength, Y_c [MPa]	113
Longitudinal shear strength, $S_{12} = S_{13}$ [MPa]	109
Peel strength, Z [MPa]	80
Transverse shear strength, S_Z [MPa]	100
Fracture energy, G_1 [kJ/m^2]	12.0
Fracture energy, G_2 [kJ/m^2]	1.0
Artificial viscosity coefficients, η_1 and η_2 [1/s]	1 (10^{-3})

$$C_{11}^0 = \frac{E_{11}(1-\nu_{32}\nu_{23})}{\Delta};\ C_{22}^0 = \frac{E_{22}(1-\nu_{31}\nu_{13})}{\Delta};\ C_{33}^0 = \frac{E_{33}(1-\nu_{21}\nu_{12})}{\Delta};$$

$$C_{12}^0 = \frac{E_{11}(\nu_{31}\nu_{23}+\nu_{21})}{\Delta};\ C_{13}^0 = \frac{E_{11}(\nu_{21}\nu_{23}+\nu_{31})}{\Delta};\ C_{23}^0 = \frac{E_{22}(\nu_{31}\nu_{12}+\nu_{32})}{\Delta};$$

$$C_{44}^0 = G_{12};\ C_{55}^0 = G_{13};\ C_{66}^0 = G_{23};$$

$$\Delta = 1-\nu_{12}\nu_{21}-\nu_{23}\nu_{32}-\nu_{13}\nu_{31}-2\nu_{13}\nu_{21}\nu_{32}$$

Given the complex state of stress/strain acting at a material point, the initial failure is predicted by applying the damage initiation criteria. The damage initiation functions f_1, f_2 and f_3 (for internal damage variables d_1, d_2 and d_3, respectively) are given by Eq. (4).

$$f_1^2 = \frac{(\epsilon_{11})^2}{\epsilon_{11}^{f,t}\epsilon_{11}^{f,c}} + \left(\frac{1}{\epsilon_{11}^{f,t}} - \frac{1}{\epsilon_{11}^{f,c}}\right)\epsilon_{11} = 1$$

$$f_2^2 = \frac{(\epsilon_{22})^2}{\epsilon_{22}^{f,t}\epsilon_{22}^{f,c}} + \left(\frac{1}{\epsilon_{22}^{f,t}} - \frac{1}{\epsilon_{22}^{f,c}}\right)\epsilon_{22} + \left(\frac{1}{\epsilon_{12}^{f}}\right)^2(\epsilon_{12})^2 = 1$$

$$f_3^2 = \left(\frac{\langle\sigma_{33}\rangle}{Z}\right)^2 + \left(\frac{\sigma_{13}}{S_z}\right)^2 + \left(\frac{\sigma_{23}}{S_z}\right)^2 = 1 \tag{4}$$

where $\epsilon_{11}^{f,t}$, $\epsilon_{11}^{f,c}$ are the failure strains in fiber direction in tension and compression, respectively; $\epsilon_{22}^{f,t}$, $\epsilon_{22}^{f,c}$ are the failure strains perpendicular to the fiber direction in tension and compression, respectively; ϵ_{12}^{f} is the failure strain in shear; Z and S_z are peel (tensile interlaminar normal) and interlaminar shear strengths, respectively. The symbol $\langle\ \rangle$ used in Eq. (4) represents the Macaulay bracket with usual interpretation. The failure strains are computed from the dividing the corresponding strengths over stiffness (assuming linear-brittle fracture). In-plane damage variables evolve monotonically in the range $0 \le d_i \le 1 (i = 1, 2)$. The evolution laws for in-plane damage variables are based on strains according to Eq. (5), where $d_i = 0$ corresponds to the initial undamaged state and $d_i = 1$ is the state of complete loss of integrity. The degradation in the through-thickness direction is assumed instantaneous, meaning there is no delamination fracture energy present in the model.

$$d_i = 1 - \frac{\epsilon_{ii}^{f,t}}{f_i} exp\left(\frac{-C_{ii}\,\epsilon_{ii}^{f,t}\,(f_i - \epsilon_{ii}^{f,t})L^c}{G_i}\right),\ i = 1, 2$$

$$d_3 = \begin{cases} 0, f_3 < 1 \\ 0.95, f_3 \ge 1 \end{cases} \tag{5}$$

wherein L^c and G_i are the FE characteristic length associated with the material point and fracture energy for the i^{th} damage variable, respectively [41]. The use of the fracture energy-based damage evolution law and the introduction of the characteristic length L^c in the damage evolution law help to minimize the mesh sensitivity of the numerical results [42], which is a common problem of constitutive models with strain softening response. The viscous regularization method [34,43] for the damage variables d_i (i = 1,2) is used to reduce damage localization and improve convergence. The strain rate dependence was introduced into the evolution law of damage variables, d_i (i = 1,2), as formulated in Eq. (5a):

$$\frac{d}{dt}(d_i^v) = \frac{1}{\eta_i}(d_i - d_i^v) \tag{5a}$$

where η_i (i = 1,2) is an artificial viscosity coefficient and d_i^v (i = 1,2) is the viscous (regularized) damage variable replacing the damage variable, d_i (i = 1,2), in the constitutive equations. To avoid unrealistic results due to viscous regularization, the associated dissipated energy should be small compared to the strain energy. The limiting factor of 0.95 for the d_3 damage variable was chosen following the general guidelines from [44].

Material constants used in the analysis are listed in Table 3.

3.4. Progressive failure analysis in a virtual tensile coupon

A virtual tensile test is performed on a PPMC coupon with dimensions of $L \times w \times t$ = 152.4 × 25.4 × 3.5 mm and the platelet dimensions of $L_p \times w_p \times t_p$ = 12.7 × 12.7 × 0.14 mm. The input OT to generate the virtual meso-morphology is 2D-random. The results of a virtual tensile test are reduced by elementary homogenization wherein the coupon effective/macroscopic response is characterized by the engineering strain, $\bar{\epsilon}_{11}$, and stress, $\bar{\sigma}_{11}$, defined as the fraction of loading displacement (i.e. coupon elongation), u_1^*, to initial length, L, and reaction force, F_1, to the cross-sectional area of a coupon, respectively. The finite-element mesh size is discussed in Appendix A1. The effect of thermal-residual stress on the composite tensile strength is discussed in Appendix A2; the thermal-residual stresses are not considered in the subsequent sections. The energy over the whole model associated with viscous stabilization methods was always less than 5% of the strain energy prior to reaching the ultimate strength.

The typical simulated evolution of macro-stress as a function of applied macro-strain, $\bar{\sigma}_{11}(\bar{\epsilon}_{11})$, is shown in Fig. 3 for several virtual coupons along with the experimental curves for the physical coupons of the similar geometrical characteristics. The simulated and experimental curves are in reasonable agreement. The strain field ϵ_{11} (x_1, x_2, x_3) is heterogeneous, as shown in Fig. 7(a) for a select virtual coupon, wherein the local strain variations result from the underlying morphology. There are regions of high and low strains, having size and

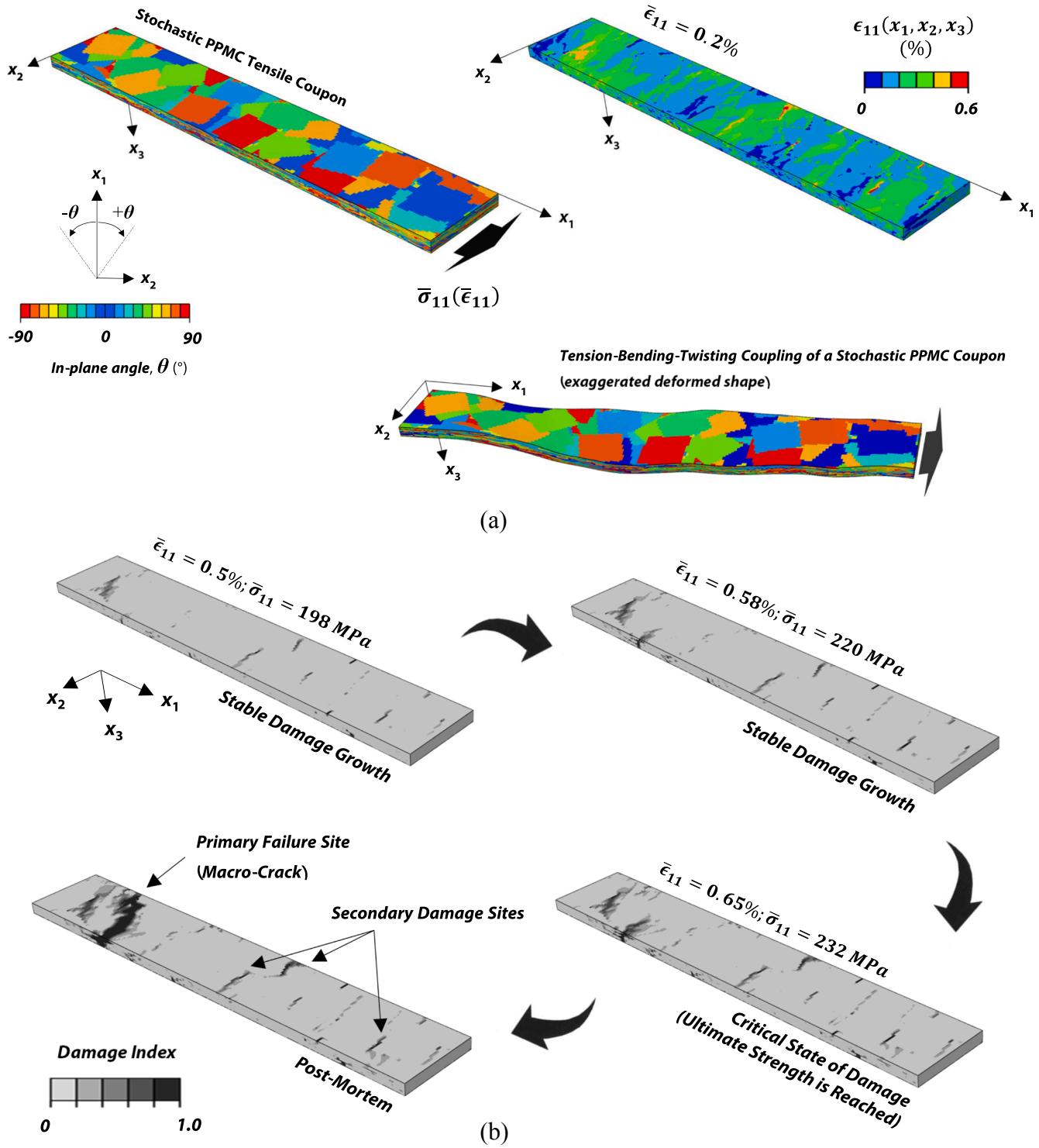

Fig. 7. (a) Demo of progressive failure analysis in a selected virtual stochastic PPMC coupon (simulation coupon #2 in Fig. 3): Distribution of elastic strains $\epsilon_{11}(x_1, x_2, x_3)$ corresponding to $\bar{\epsilon}_{11} = 0.2\%$ and tension-bending-twisting coupling under uniaxial tension of a coupon; (b) Stages of damage progression, wherein damage index is $d = max\{d_i\}_{i=1}^{3}$. (For interpretation of the references to colour in this figure legend, the reader is referred to the web version of this article.)

shape relevant to the (*i*) local orientation state and (*ii*) global deformation of a coupon. High local strains are visible on the coupon surface at locations where platelets are less aligned with the loading direction (x_1). The strain field has gradients in a coupon through-thickness direction due to local changes in stiffness from local variations in platelet orientations. Variable local stiffness in a tensile coupon makes a position of the shear center and a non-coincident centroid vary between the cross sections along the coupon length. Non-symmetric distribution of geometrical and local material properties (from local orientations) causes mechanical coupling between different modes of deformation. Fig. 7 (a) illustrates the bending-twisting-extension coupling that may arise in a stochastic PPMC tensile specimen, where the deformation is scaled by a factor of ten to highlight out-of-plane displacements resulting from uniaxial tension. Irregularity of the meso-scale morphology of a PPMC gives rise to gradients in the platelet-level in-plane stress fields even during the macroscopic tensile deformation.

In-plane stress gradients give rise to the inter- platelet ("interlaminar") stresses [46], which are developed when there are discontinuities in the load path, e.g. such as platelet edges, and drive the delamination (separation) between different platelets stacked together in a composite system. The simulation provides the description of interactions of inherent stress concentrations, which lead to the complex damage pattern caused by internal characteristics of stochastic meso-morphology.

A PPMC experiences multiple local failures, wherein local meso-scale cracks grow and arrest prior to macroscopic coalescence and global failure. Fig. 7(b) shows the complex pattern of coupled failure mechanisms and stages of progressive damage in the meso-structure of a PPMC coupon. The path of damage in the simulation is represented by the patterns (distributions) of the corresponding damage variables, which reflect the state of degradation of local stiffness responsible for local loss of stress carrying capacity and thus representing "smeared" local meso-scale cracks. In Fig. 7 (b), the undamaged and damaged regions within a coupon domain are obtained from the FE solution and are identified by the light gray ($d = 0$, no crack) and solid black ($d = 1$, local crack) colors, respectively, wherein d is the maximum damage index, $d = max\{d_i\}_{i=1}^{3}$. Prior to damage initiation (and even under "little" damage), the effective stress–strain response, $\bar{\sigma}_{11}(\bar{\varepsilon}_{11})$, is linear-elastic. The transverse and through-thickness damage modes are first to appear. After damage initiation, the platelet meso-structure starts developing the damage process zone (DPZ), which is an accumulation of growing and coalescing damaged local regions. Internal redundancy of the PPMC meso-structure allows it to redistribute the applied load to undamaged elements (regions surrounding the damaged spots) when localized material softening develops. As the damage seeks for alternative paths for progression, the meso-structure develops multiple simultaneous precursory damage sites. With the incipience of the DPZ, the load-carrying capacity of the composite is reduced and the coupon stress-strain relationship, $\bar{\sigma}_{11}(\bar{\varepsilon}_{11})$, exhibits non-linear behavior. As the loading is increased, the damage matures and builds up throughout the composite volume. The DPZ propagates (grows) in a stable manner until a *critical amount of damage* is accumulated and *ultimate strength* is reached, thereafter an unstable propagation of damage happens signifying the final ultimate failure of a coupon. The longitudinal (fiber direction) damage may take place at that stage. Fig. 8 shows the distribution of individual damage variables in the post-mortem of a selected coupon, which allows to interpret the macro-crack as a combination of all three meso-scale damage modes. The secondary damage sites (combinations of interlaminar and intralaminar failure modes) can be observed in Fig. 8 as well. At the macroscopic scale, failure of a coupon is associated with its "separation" in two pieces by a macro-crack and is preceded by the formation of a band from local damage precursors where most of the damage activity accumulates (see Figs. 7 and 8).

The regions of high strain are the regions where damage develops in the first place. It seems that the major and most of the minor failure sites are located where the coupling between deformation modes is the most prominent, close to the convex and concave surfaces of a coupon. Additionally, the damage tends to initiate near the edges of a coupon close to those locations. An interesting observation is that the location of the early damage in the loading history does not have to appear as the prominent ultimate failure site, see Fig. 7(b).

3.5. Statistical validation of probabilistic distribution of stochastic PPMC tensile properties from in-silico test series

In the presence of uncertainty, such as "random" spatial overlaps and variability of local orientations of platelets within coupons, the measured macroscopic PPMC tensile properties are non-deterministic in nature. Explicitly modeled heterogeneous meso-structure in virtual coupons allows quantification of the mechanical properties distribution of a stochastic PPMC, which emanates from the variability in the meso-scale morphologies. Twenty virtual coupons were individually generated by requesting a 2D-random OT to simulate the stochastic tensile properties of 3.5 mm thick PPMC coupons made of $12.7 \times 12.7 \times 0.14$ mm ($L_p \times w_p \times t_p$) platelets.

Experimental and simulation results of coupon stiffness and strength scatter are compared in Fig. 9 (a). Fig. 9 (b, left) shows strength plotted versus stiffness of the experimental and virtual coupons. Stochastic PPMCs exhibit local orientation variability on sufficiently large length scales, despite maintaining the same nominal global orientation state. The local variability of meso-scale morphology translates into *both* the variability of effective tensile stiffness and strength. The local variations of the stochastic orientation state produce the effect of "springs-in-series", which explains the sensitivity of the macroscopic stiffness to the

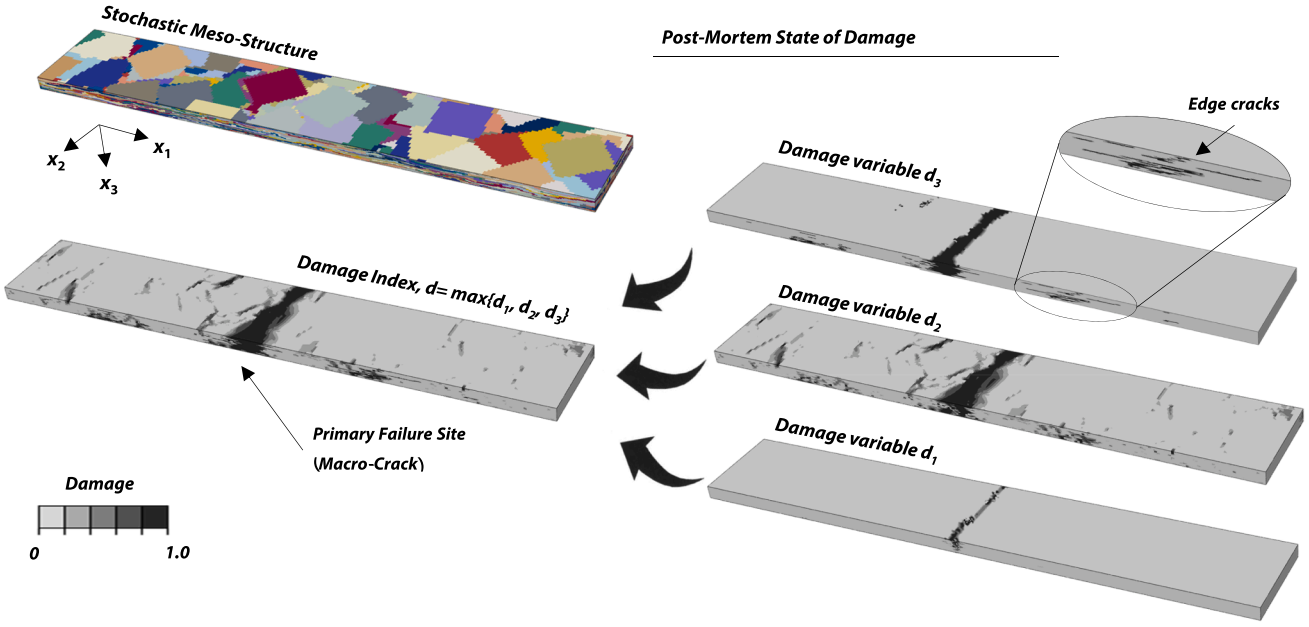

Fig. 8. Distribution of different damage variables (d_1, d_2, d_3) and the local maximum (d) in the post-mortem of a selected coupon. (For interpretation of the references to colour in this figure legend, the reader is referred to the web version of this article.)

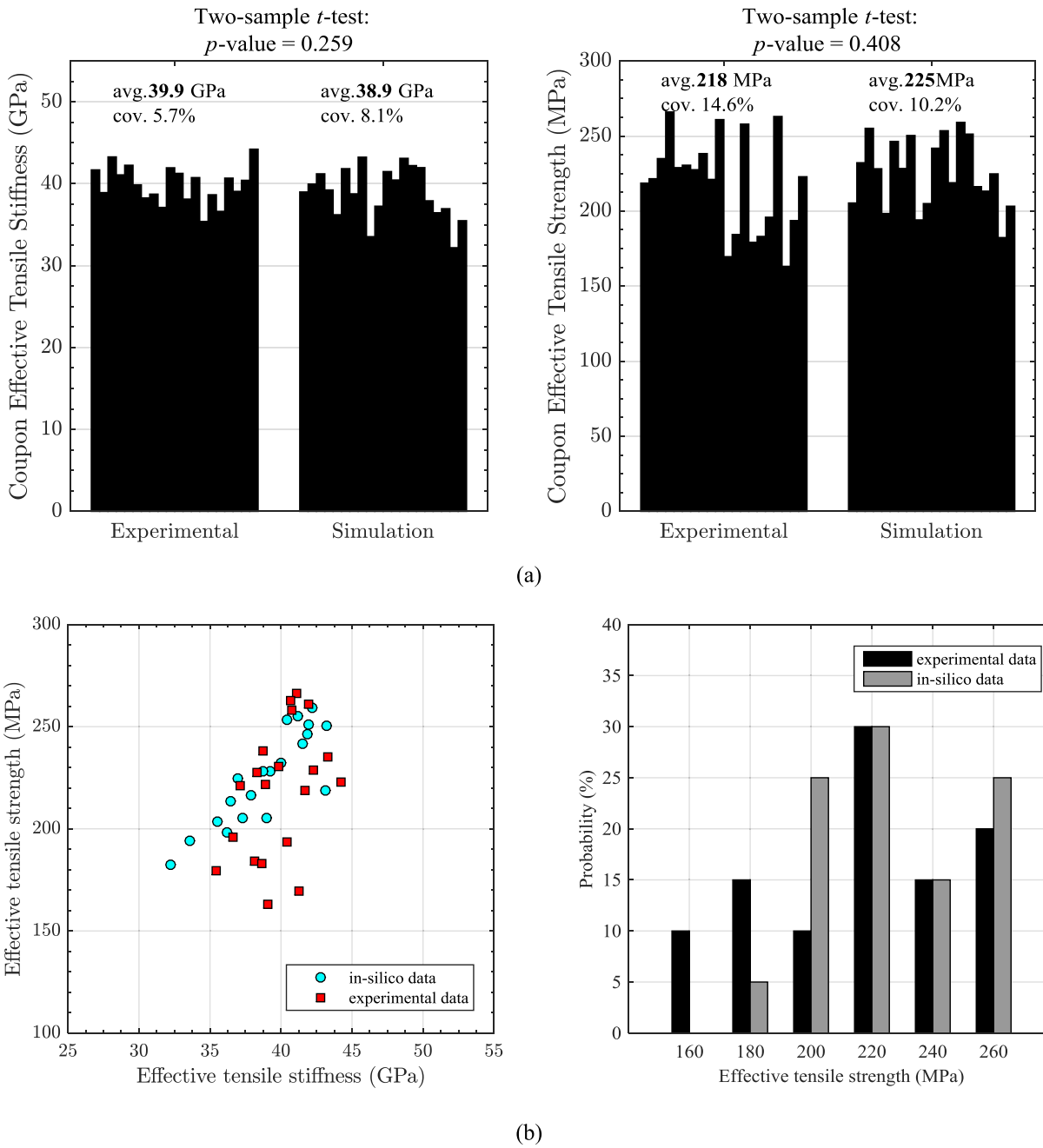

Fig. 9. (a) Variability of effective tensile stiffness and strength in a stochastic PPMC made of 12.7 × 12.7 mm ($L_p \times w_p$) platelets: experimental and simulated, coupon thickness ~3.6 mm; (b) Stiffness-strength correlation (left) and discrete probability distribution of tensile strength (right) in physical and virtual tensile coupons. (For interpretation of the references to colour in this figure legend, the reader is referred to the web version of this article.)

details of local meso-morphology. The strong influence of local effects of stochastic meso-morphology is best reflected in the poor correlation between the macroscopic stiffness and strength of PPMC coupons. As data in Fig. 9 (a, on the left) shows, the coupons with nearly the same stiffness may exhibit different strength values, and inversely the coupons possessing different stiffness may have nearly similar strengths.

The histogram in Fig. 9 (b, on the right) specifies the probability of stochastic strength over its range of values. The discrete probability distributions of the experimentally measured values and the outcomes of the in-silico tests appear to be in a reasonable agreement, except for the likelihood of obtaining the possible lowest values of PPMC stochastic strength. Validation of the results of probabilistic simulation of stochastic PPMC tensile properties is performed by comparing the experimental and in-silico property distributions by the two-sample *t*- and K-S tests, wherein the null hypothesis claims that there is no difference between the distributions. The two-tailed *p*-value between the mean scores obtained from the probabilistic virtual and experimental test series from the two-sample *t*-test is 0.259 between the stiffness data samples and 0.408 between the strength data samples. Both *p*-values are greater than 0.05, so the null hypothesis cannot be rejected at the 5% SL. The cumulative distributions, indicating the probability of a variable being less or equal to a specified value, of stiffness and strength are shown in Fig. 10. The CDFs appear to agree well by visual comparison. The statistic of the K-S test (supremum $D = 0.25$) is associated to a p-value = 0.497, which indicates that the two distributions are not significantly different at the 5% SL. Therefore, the difference in results between the two data samples (experimental and simulated) is deemed *not* being statistically significant. This means that the simulation and

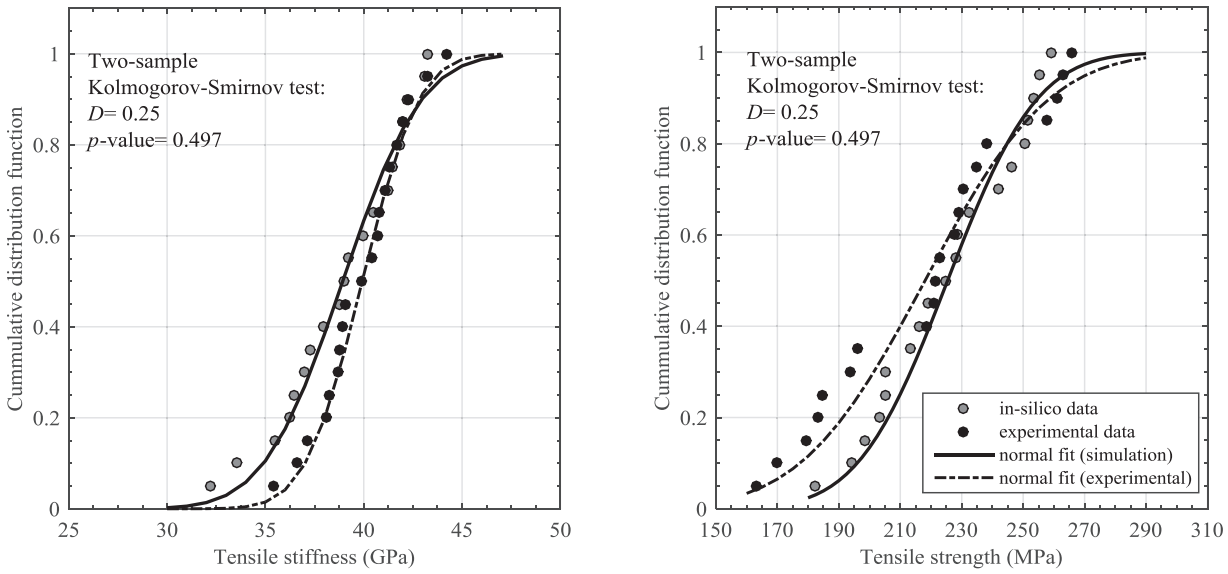

Fig. 10. Cumulative distributions of stiffness and strength from experimental and in-silico tests.

experimental results can be thought to belong to the same underlying population, implying that the simulation results can be considered reliable.

4. Computational analysis of the structure-property relationship in a stochastic PPMC under uniaxial tension

4.1. Simulated coupon thickness effect on the properties of a stochastic PPMC

The present section demonstrates that for a given platelet size, the increased thickness of a tensile coupon provides for the improved average and reduced variability of stochastic PPMC effective properties. This phenomenon is a manifestation of the effect of increased platelet count as stochastic PPMC coupons with more platelets exhibit less dissimilarity in the meso-morphology descriptors, both in the local and global sense (for reduced variability) and have more internal redundancy and better chances for a more uniform orientation state with fewer "weak" spots (for improved properties). The analysis of statistical significance of the simulated results suggests that the dependence of stochastic PPMC effective properties on coupon thickness must have a limit when properties saturate and show no further increase beyond a specific coupon thickness.

To evaluate the effect of coupon thickness on PPMC tensile properties, four batches of stochastic virtual coupons with platelet dimensions of $L_p \times w_p \times t_p = 12.7 \times 12.7 \times 0.14$ mm were generated, with coupon thicknesses of 1.4, 2.38, 3.5, and 6.44 m. Fig. 11(a) shows a view on coupons and their dimensions. The stochastic orientation state in individually generated virtual coupons is modeled after the nominal "2D-random" second order OT. Each batch with given coupon thickness had ten specimens in it. Strength and modulus vary from one coupon to another due to inherent morphological dissimilarities. The simulated tensile properties of PPMC coupons are summarized in the bar charts in Fig. 11(b). Improved effective stiffness and strength and reduced variability is seen for the thicker stochastic coupons. The distributions of in-silico tensile properties are subjected to the two-sample statistical tests to determine if the variation of composite thickness has a statistically significant effect on properties. The p-values from the two-sample t- and K-S tests are reported in Table 4 and are used to test the null-hypothesis stating that the samples represent the same distribution. The results of the *t*-test show that there is a strong (statistically significant) difference between the mean tensile properties of the 1.4 and 2.38 mm thick coupons at the 5% SL, as the p-values for the two batches for both stiffness (2.5%) and strength (0.24%) are less than 5%. The difference in mean strength between the 2.38 and 3.5 mm thick coupons can be considered significant at the 10% SL as the p-value is 7%. The p-value of 38% for strength and 45% for stiffness draws the conclusion that the data from the 3.5 and 6.44 mm thick coupons cannot be considered to have significantly different means at either 5 or 10% SL. The means of the stiffness and strength distributions are significantly different between the 1.4 and 3.5, and 2.38 and 6.44 mm thick coupons at the 5% SL. The p-values from the statistic of the K-S test (Table 4) indicate that the CDFs of the stiffness and strength of the 1.4 and 2.38 mm, 1.4 and 3.5 mm, and 2.38 and 6.44 mm thick coupons are significantly different at the 5% SL.

Internal variability of (local) orientation state is more pronounced in thinner coupons as compared to the thicker coupons. Fig. 12 compares the measures of local and global alignment of the stochastic orientation state in five arbitrarily selected coupons of two thicknesses, $t = 1.4$ and 3.5 mm. A thicker virtual tensile coupon (average 940 platelets/coupon) encompasses a greater number of platelets than a thinner coupon (average 340 platelets/coupon). Even with a random placement procedure based on the generation of pseudo-random numbers after the uniform distribution (for platelets centroids and orientations), the increased number of platelets in a virtual tensile coupon results in the mitigation of statistical difference between the individual coupons. When uniform distribution is used to generate the virtual coupons, thinner coupons are more statistically different from one other than the thicker coupons. The resulting average a_{11} between the five thin coupons is 0.4896 with a coefficient of variance (cov) of 5%, while the average a_{11} between the five thick coupons is 0.50 with a substantially lower cov of 0.75%. This explains the reduced variance of effective stiffness and strength in thicker coupons as compared to the thinner coupons. Let us now use the same a_{11} entry of the second order OT to quantify the local degree of platelet alignment in six (1in) × (1in) × (coupon thickness) volumetric sub-domains (V_i) within a single virtual tensile coupon, see Fig. 12. A smaller number of generated platelets as in a thinner tensile coupon results in two things: (*i*) a greater variance of local orientation state, and (*ii*) possibility of achieving a lower local degree of alignment, as compared to the case of a thicker coupon. The former and latter provide for the reduced effective stiffness and strength. In other words, for a smaller platelet count, the chances of having a local drastically dissimilar orientation state in a stochastic meso-structure (like a "weak spot") are higher, while the increased platelet count leads to the improved uniformity of the local orientation state. In general, by the empirical observations, large

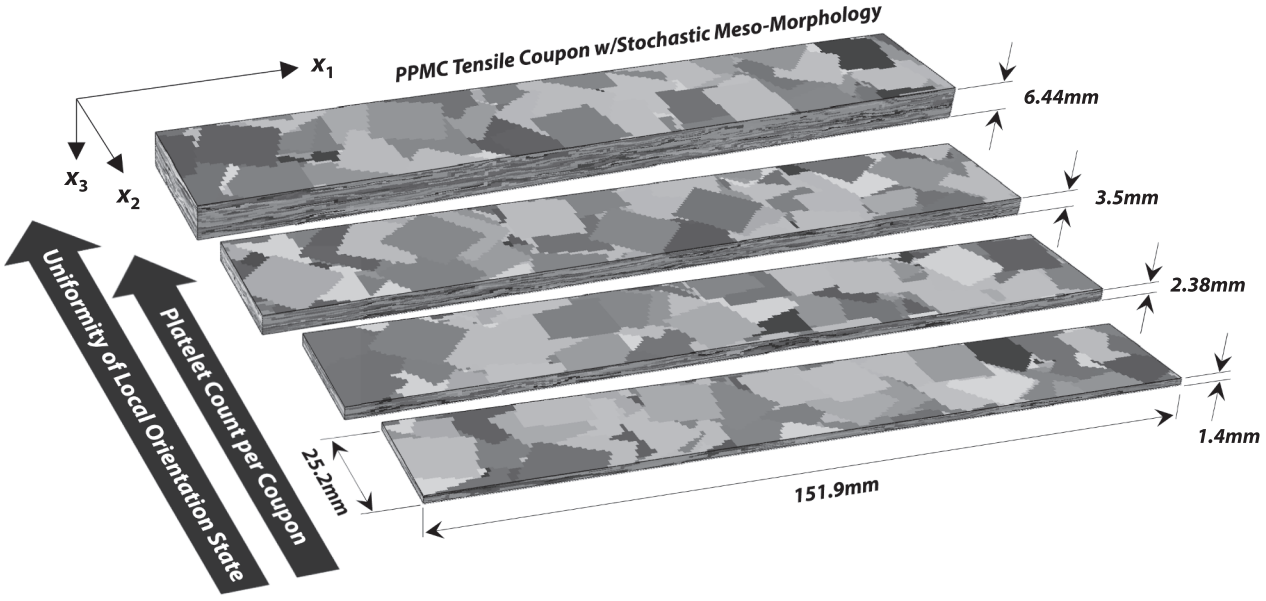

(a)

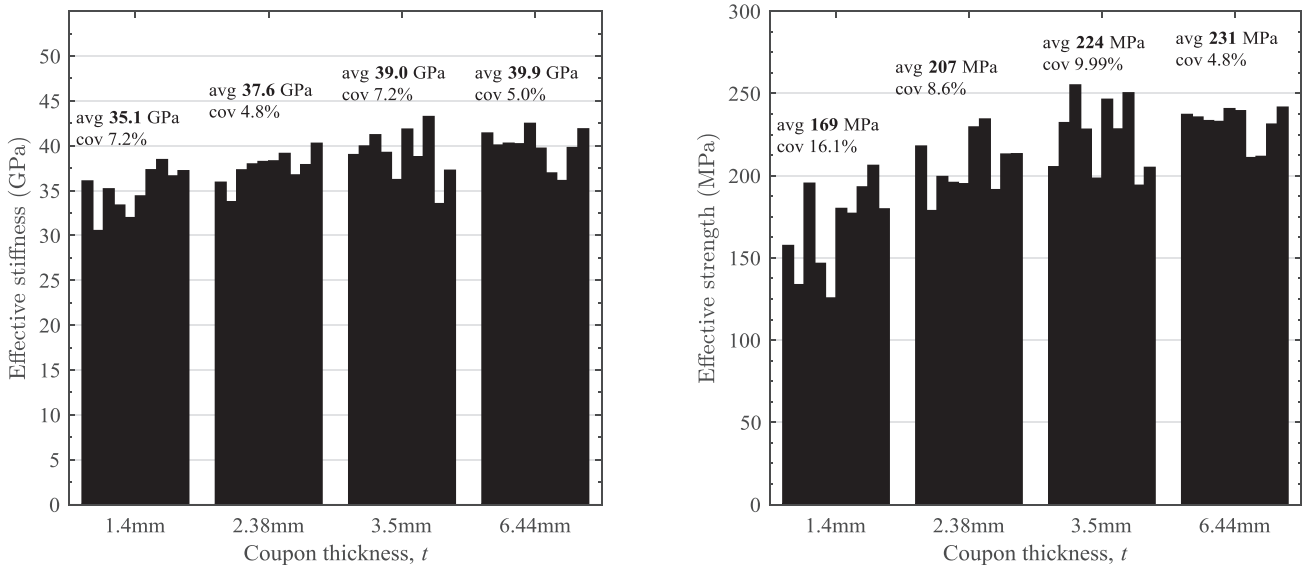

(b)

Fig. 11. (a) Virtual PPMC coupons of variable thickness (t) made of platelets with $Lp \times w_p \times t_p = 12.7 \times 12.7 \times 0.14$ mm, prepared for the in-silico tensile testing (along the x_1-direction); (b) Stiffness and strength vs coupon thickness (in-silico test results). Stochastic morphology generated after requested uniform ODF.

random samples drawn from any distribution will tend to look like the distribution they are taken from. Following the "Law of Large Numbers", the local variability of the orientation state in a virtual PPMC coupon would smear out to become more "uniform" (if the uniform ODF was used to sample the random numbers) at a substantially large platelet count.

The results of probabilistic computational analysis of the effect of coupon thickness on PPMC stochastic tensile properties support the experimental observations of the Section 2.4. Fig. 13 shows the box-and-whisker diagram displaying the distribution of experimental and simulated strength through their quartiles. Two-sample t- and K-S tests indicate that the in-silico and experimental strength distributions for 1.4, 3.5, and 6.44 mm thick coupons are not significantly different at the 5% significance level. The narrow interquartile range of the in-silico strength distribution of 6.44 mm-thick coupons (as compared to the experimental range) stems from the saturation of the local orientation states in virtual coupons caused by the large number of realizations of the pseudo-random number generator. Saturation/"uniformity" of local orientation states in virtual coupons apparently happens at a lower platelet count (as compared to the physical reality), due to the inherent limitations of PRNG to approximate stochasticity.

4.2. *Effect of the meso-scale orientation state on the properties of a stochastic PPMC*

This section investigates the tensile properties of PPMC meso-structures having stochastic orientation states with variable degree of global alignment of platelets with the loading direction. "Preferentially oriented platelets" does not mean perfect alignment, as there is always a distribution of orientations in a stochastic meso-morphology. Virtual

Table 4
Statistical analysis of variation of PPMC tensile properties with coupon thickness, obtained in-silico. Platelet size $L_p \times w_p \times t_p = 12.7 \times 12.7 \times 0.14$ mm, stochastic morphology generated after requested uniform ODF.

(a)

Coupon avg. thickness (mm)	Sample size	Tensile Stiffness (In-Silico)						Tensile Strength (In-Silico)					
		Avg. (GPa)	St. Dev. (GPa)	COV(%)	*p*-value			Avg. (MPa)	St. Dev. (MPa)	COV(%)	*p*-value		
					A-D test	*t*-test	K-S test				A-D test	*t*-test	K-S test
1.40	10	35.12	2.54	7.2	0.7454			169.5	27.3	16.1	0.5194		
2.38	10	37.55	1.79	4.8	0.5218	0.0245	0.111	206.9	17.7	8.6	0.7472	0.0024	0.031
3.50	10	39.03	2.84	7.3	0.9309	0.1835	0.111	224.4	22.4	9.9	0.3459	0.070	0.313
6.44	10	39.89	2.01	5.0	0.1511	0.4467	0.313	231.8	11.2	4.8	0.0075	0.3847	0.313

(b)

Compared samples (coupon thickness)	Stiffness (In-Silico)		Strength (In-Silico)	
	Two sample *t*-test: *p*-value	Two-sample K-S test: *D* – statistic/ *p*-value	Two sample *t*-test: *p*-value	Two-sample K-S test: *D* – statistic/ *p*-value
1.4 mm vs 3.5 mm	0.0045	0.7/0.0069	1.26 (10^{-4})	0.8/0.0012
2.38 mm vs 6.44 mm	0.0133	0.7/0.0069	0.002	0.7/0.0069

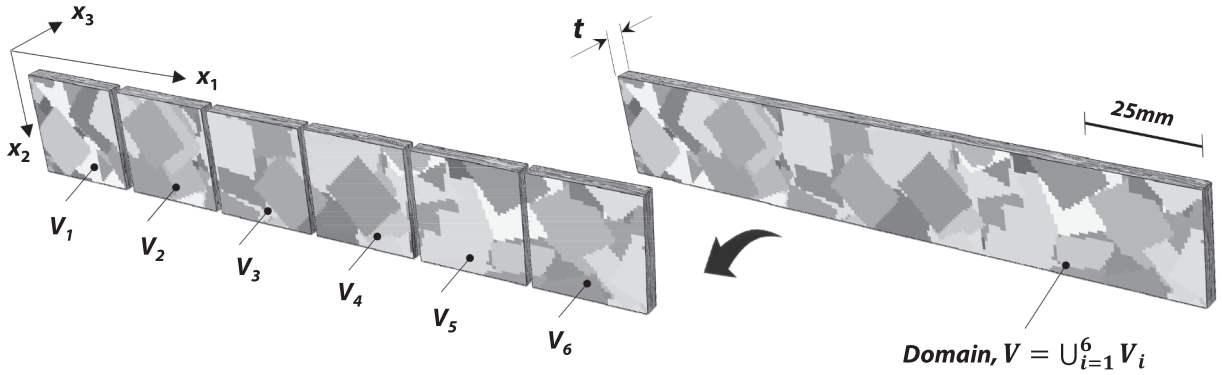

(a)

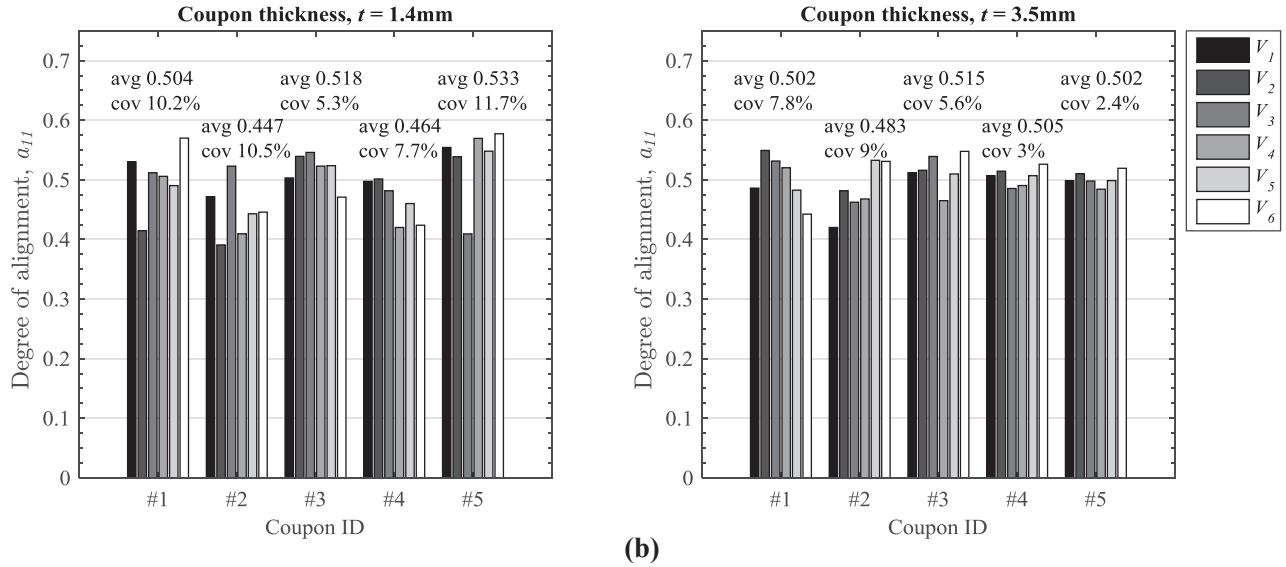

(b)

Fig. 12. Regional analysis of the degree of alignment $a_{11} = \frac{1}{N}\sum_{k=1}^{N}\cos^2\theta_k$ (N is the number of platelets) in volumetric subdomains V_i comprising the domain V occupied by a virtual coupon with stochastic meso-morphology (for five selected coupons of two thicknesses). All virtual coupons are generated by sampling the platelet orientation angles from the uniform ODF.

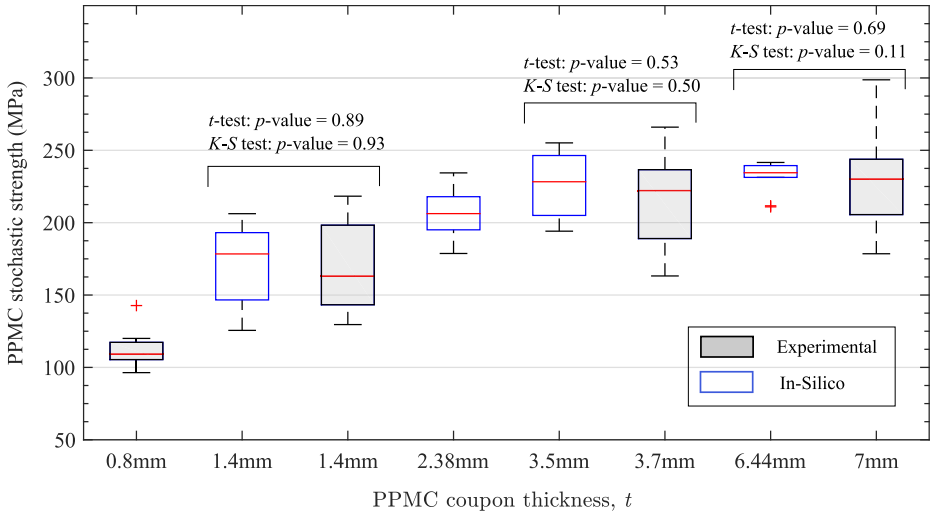

Fig. 13. Box-and-whisker plot of strength data as a function of PPMC coupon thickness, experimental and simulated (platelet $L_p \times w_p = 12.7 \times 12.7$ mm, platelet thickness in in-silico coupons $t_p = 0.14$ mm). (For interpretation of the references to colour in this figure legend, the reader is referred to the web version of this article.)

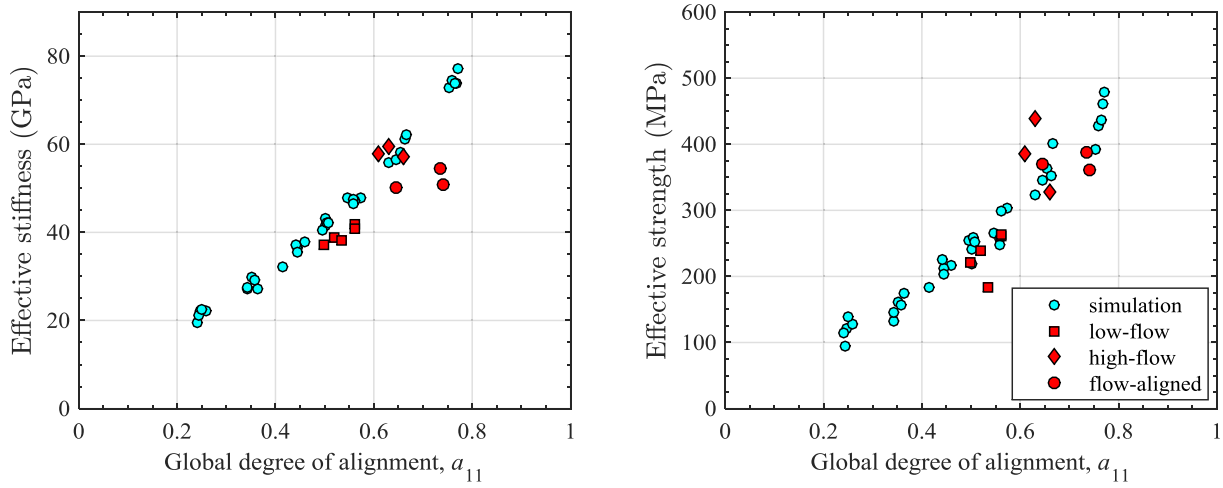

Fig. 14. PPMC effective tensile stiffness and strength as a function of global degree of platelets alignment in coupons with stochastic morphology ($L_p \times w_p = 12.7 \times 12.7$ mm). (For interpretation of the references to colour in this figure legend, the reader is referred to the web version of this article.)

tensile coupons were generated to have a global degree of platelets alignment, a_{11}, in the range between 0.25 and 0.75, with $a_{22} = 1 - a_{11}$ and other terms of the second order orientation tensor (OT) to be zero. A greater a_{11} implies more platelets having their fiber direction more aligned with the global x_1-direction. The coupon in-plane dimensions were as in the previous section and coupon thickness was 3.5 mm. The platelet dimensions were $L_p \times w_p \times t_p = 12.7 \times 12.7 \times 0.1$ mm. Simulation showed that substantial gains in the tensile properties of a PPMC can be achieved by introducing platelet alignment in the loading direction. The results of the in-silico tensile testing of all coupons are summarized in Fig. 14, where effective stiffness and strength of PPMC coupons are plotted vs the global (all-coupon) degree of alignment. The coupons with a greater degree of platelets alignment have a greater fraction of finite elements with damage variable $d_3 \neq 0$ and a smaller fraction of elements with $d_3 = 0$, identifying the increased probability of local delamination appearance. The increased tensile properties of coupons with a greater degree of platelets alignment with the loading direction is explained by the increased local off-axis strength of platelet material. Fig. 14 also reports the experimentally measured stiffness and strength versus the CT-measured degree of global platelet alignment. A reasonable correlation between the simulated (in-silico) and experimental results stems from the results presented in Fig. 14.

4.3. Effects of platelet geometry on the properties of a stochastic PPMC

The goal of this section is to analyze how the variation of platelet length (L_p) and thickness (t_p) affect the distributions of stochastic PPMC tensile properties. When a platelet length-to-thickness ratio, L_p/t_p, is increased, the meso-scale stress transfer between platelets becomes more efficient and composite macroscopic/effective properties are improved. Changed platelet dimensions in a fixed volume of a PPMC coupon alter the platelet count, which has a strong effect on the local variability of composite meso-morphology. Increased platelet length in the same size coupon with stochastic meso-morphology decreases the platelet count and provides for enhanced statistical dissimilarity between individual coupons, which translates into more scattered composite macro-properties. Decreased platelet thickness in the same size coupon increases the platelets count and, consequently, favors the mitigation of meso-morphology dissimilarity between individual stochastic PPMC coupons, which implies reduced variability of composite properties.

4.3.1. Understanding the effect of improved stress sharing between platelets on the effective properties of a PPMC

In the previous work [47], it was systematically shown for a system of aligned platelets that an increased platelet slenderness (length-to-thickness ratio, L_p/t_p) suppresses delaminations between the platelets and allows platelets to acquire more in-plane stress before system

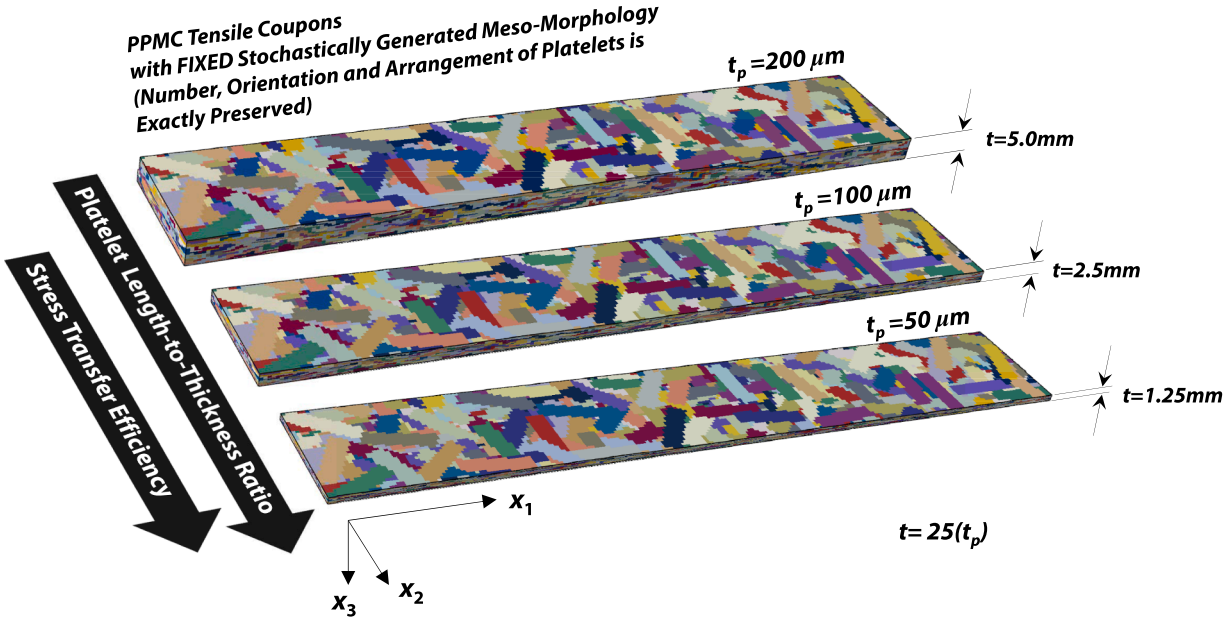

(a)

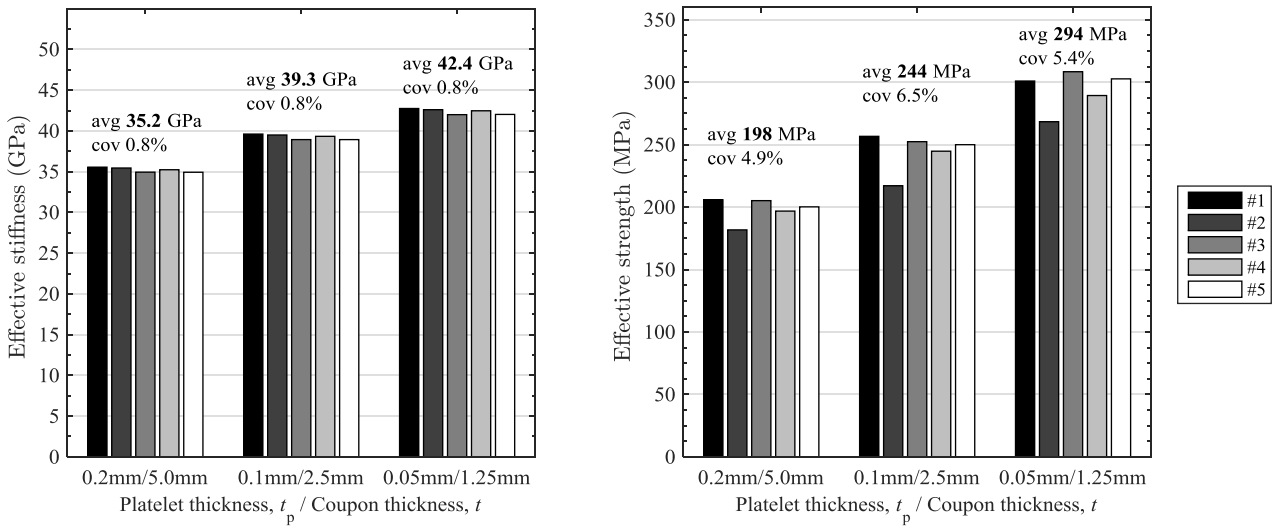

(b)

Fig. 15. Effect of platelet length-to-thickness (L_p/t_p) ratio on the effective tensile properties of a stochastic PPMC. Five coupons (##1-5) with stochastically generated meso-morphology (after uniform ODF), fixed for different platelet thickness; platelet length, L_p = 12.7 mm (L_p/w_p = 4). (For interpretation of the references to colour in this figure legend, the reader is referred to the web version of this article.)

ultimate failure, thus promoting a more efficient stress transfer within a system. The mechanisms for stress transfer from platelet to platelet are similar in a PPMC system with multiple platelet orientations. It was possible to consider the same arrangement of aligned platelets when the platelet length and thickness were varied independently but yield the same L_p/t_p-ratio, to draw a conclusion that it is a platelet length-to-thickness ratio controls the stress transfer efficiency. It is though not possible to change the platelet length in a stochastic (multi-directional) PPMC and preserve the platelets arrangement, but it is possible to change the platelet thickness and preserve the meso-structure architecture (morphology).

Five full-size virtual PPMC coupons with stochastically generated meso-morphology were tested in-silico for the tensile stiffness and strength. Stochastic orientation state was sampled from a uniform ODF. Each meso-morphology within a coupon was reproduced for the three platelet thicknesses, t_p, of 50, 100, and 200 μm, while the orientations and geometrical arrangement of platelets were exactly the same. This was achieved by keeping the random seed constant when exercising the pseudo-random number generation algorithm to construct a given stochastic meso-morphology. The platelet length (L_p) and width (w_p) were 12.7 and 3.175 mm, respectively. In other words, a given meso-morphology was "swelled" (scaled in the coupon thickness, x_3-direction) as the platelet thickness was increased, as shown in Fig. 15(a). By considering the replications of the fixed stochastically generated meso-morphology with the platelets of various L_p/t_p-ratios, we isolate the effects of morphology from the effect of platelet geometry on the effective PPMC properties.

Fig. 15(b) shows that the increased platelet L_p/t_p-ratio improves the effective stiffness and strength in each PPMC coupon with stochastically generated meso-morphology. A coupon with thinner platelets has a

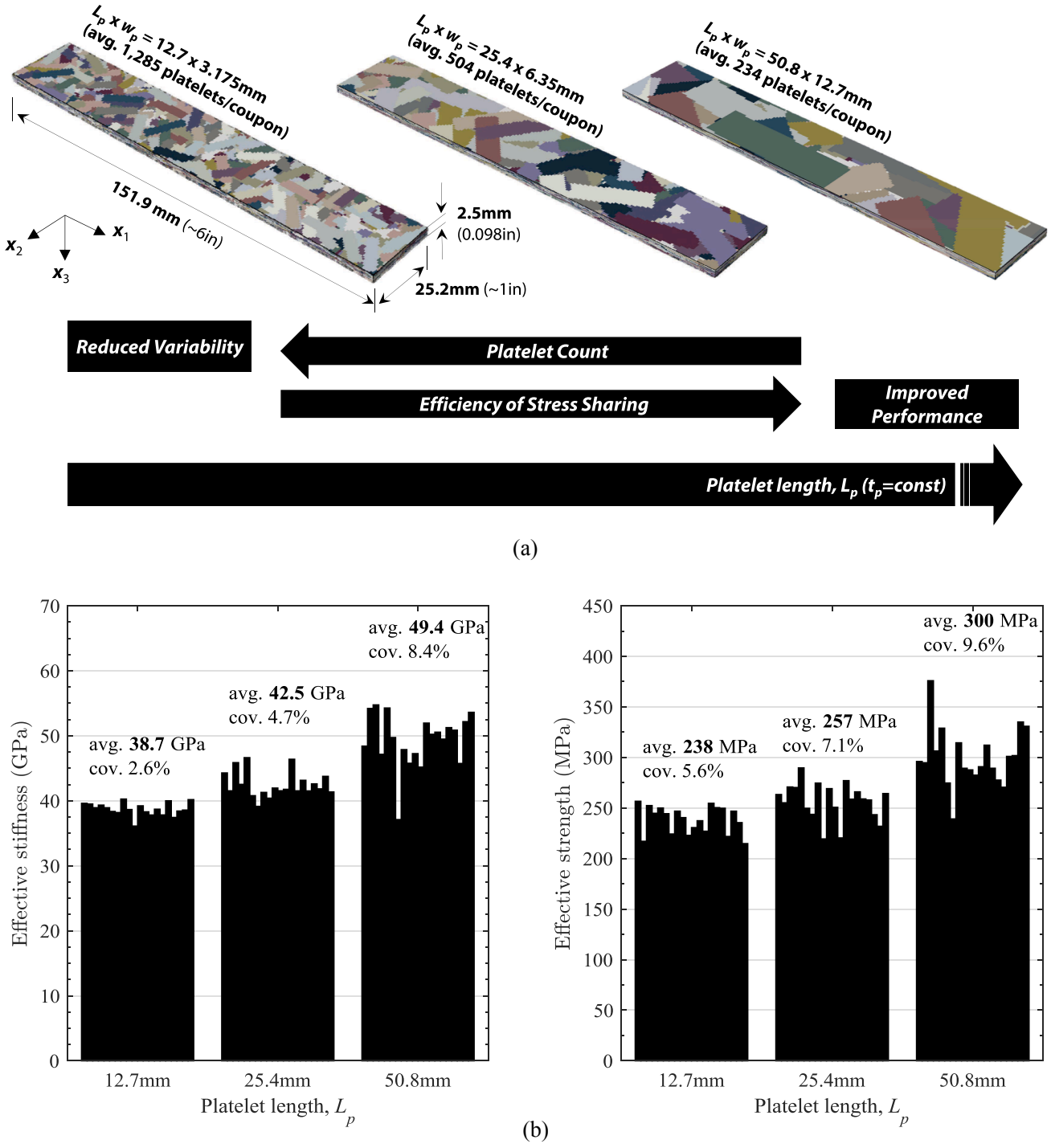

Fig. 16. Probabilistic effect of platelet length on effective tensile properties of a stochastic PPMC: (a) Virtual meso-structures for in-silico tensile testing; (b) Results of in-silico tensile test series. Platelet thickness, t_p = 0.1 mm; stochastic meso-morphologies generated by requesting a uniform ODF. (For interpretation of the references to colour in this figure legend, the reader is referred to the web version of this article.)

greater number of finite elements with $d_3 = 0$ and a smaller number of finite elements with $d_3 = 0.95$ compared to the case of a thicker platelet, i.e. thinner platelets cause less delaminations. The reduced statistics of the "delamination" damage variable and the increased effective strength allow to suggest that a greater platelet L_p/t_p-ratio is responsible for the improved stress transfer within a PPMC with stochastic meso-morphology.

4.3.2. Probabilistic effect of platelet length on composite stochastic tensile stiffness and strength (coupons of constant thickness)

The present section investigates how the platelet length (L_p) probabilistically defines the macroscopic tensile properties of a stochastic PPMC. The digital coupons had fixed dimensions of length (L), width (w), and thickness (t) of 152.4 mm, 25.4 mm, 2.52 mm, respectively, and were made of the platelets having three different lengths, L_p = 12.7, 25.4, and 50.8 mm while the platelet thickness was set to 0.1 mm. The platelet length-to-width ratio, L_p/w_p, was equal to four. The stochastic orientation state of meso-morphology was generated

Table 5
Statistical analysis of variation of PPMC tensile properties with platelet length for a given coupon thickness, obtained in-silico. Platelet thickness, t_p = 0.1 mm; coupon thickness, t = 2.5 mm; stochastic morphology generated after requested uniform ODF.

Platelet length (mm)	Sample size	Tensile Stiffness (In-Silico)						Tensile Strength (In-Silico)					
		Avg. (GPa)	St. Dev. (GPa)	COV(%)	*p*-value			Avg. (MPa)	St. Dev. (MPa)	COV(%)	*p*-value		
					A-D test	*t*-test	K-S test				A-D test	*t*-test	K-S test
12.7	20	38.72	1.00	2.59	0.810			238.45	13.28	5.57	0.123		
25.4	20	42.49	1.99	4.68	0.013	$4.4\ (10^{-4})$	$4.7\ (10^{-9})$	256.77	18.23	7.10	0.384	$1.5\ (10^{-8})$	$7.3\ (10^{-4})$
50.8	20	49.38	4.13	8.36	0.274	$1.4\ (10^{-6})$	$1.5\ (10^{-6})$	299.96	28.75	9.58	0.286	$1.6\ (10^{-7})$	$1.5\ (10^{-6})$

after the uniform ODF by nominally requesting the 2D-random a_{ij}. Twenty virtual coupons were tested in-silico for tensile stiffness and strength for each platelet length. Fig. 16 (a) provides the representative view on the coupons, while Fig. 16(b) summarizes the simulated distributions of effective tensile properties. With the platelet length increased, the average stiffness and strength also increase, but so does the variability. All data samples showed no significant departure from normality at the 5% SL, as the *p*-values of the Anderson-Darling normality tests are greater than 0.05 (Table 5). The *p*-values associated with the two-sample *t*- and K-S tests indicate that the mean values and the distributions of PPMC stiffness and strength for the considered platelet lengths are significantly different at the 5% SL (Table 5). Therefore, it can be concluded that the platelet length has a statistically significant effect on tensile properties of a stochastic PPMC.

The improved effective properties for the coupons with longer platelets are explained by the enhanced stress sharing between platelets with greater L_p/t_p-ratio. With longer platelets, the fraction of finite elements with $d_3 = 0$ is increased and the fraction of finite elements with $d_3 = 0.95$ is reduced in coupons as compared to the case of shorter platelets, indicating the reduced probability of local delaminations appearance. The reduced inter-platelet damage provides for increased composite tensile properties. The increased variability is explained by the interference of scales between a platelet and a coupon, meaning that a longer platelet implies a smaller number of platelets in a coupon, compare 1285, 504, and 234 platelets/coupon on average for the platelet lengths of 12.7, 25.4, and 50.8 mm, respectively. Therefore, the meso-morphologies of individual coupons with longer platelets are statistically "more different" from one another, with less uniformity of local orientation states. Even though the internal redundancy of the meso-structure with longer platelets is reduced by the reduced platelet count, the superior stress transfer allows it to achieve greater effective tensile properties.

4.3.3. Probabilistic effect of platelet thickness on composite stochastic tensile stiffness and strength (coupons of constant thickness)

Herein, the fixed size virtual tensile coupons have the same dimensions as in the preceding section. The coupons are generated after the 2D-random a_{ij}. The virtual coupons of the same thickness are made of platelets with length L_p = 50.8 mm (2in) for the three values of platelet thicknesses, t_p, namely 50, 100, and 250 μm, as shown in Fig. 17(a). Five digital coupons for each platelet thickness were tested in-silico to collect the PPMC macroscopic tensile stiffness and strength data, which are summarized in Fig. 17(b). Improved mean values of properties with reduced variability for coupons with thinner platelets are seen from the in-silico data. This is due to the increased platelet (L_p/t_p)-ratio and increased platelets count in the coupons with platelet thickness decreased. Increased platelet aspect ratio improves stress transfer between platelets. A greater number of platelets allows for (*i*) a more uniform local orientation state (reduced variability of local morphology) for the reduced variability in effective properties and (*ii*) enhanced internal redundancy to benefit the strength properties.

4.4. Discussion: meso-structure descriptors and macroscopic tensile properties of a stochastic PPMC

Complex meso-scale structural interactions take place during tensile deformation of a stochastic PPMC, leading to extensive redistributions of loads during the formation of the spread out damage patterns. As this behavior results from interactions between the platelets as an ensemble, it is helpful to summarize the links between the effective composite properties and the descriptors of the composite meso-structure. Emergence of the effective PPMC properties from the underlying meso-structure is nontrivial, and some of the trends investigated in the foregoing sections are schematically summarized in Fig. 18 and further discussed in more detail. Platelet count, geometrical arrangement and geometrical parameters of platelets, and the orientation state within a composite lay foundation to effective performance of a PPMC.

The geometrical arrangement and parameters of platelets define the efficiency of stress transfer within a composite, meaning the ability of platelets to acquire more stress in the fiber direction and suppressing the interlaminar stresses thus contributing more into the macroscopic composite properties. During the macroscopic tensile deformation of a PPMC, the stochastic semi-laminated meso-structure develops gradients in the platelet-level in-plane stresses (σ_{11}, σ_{22}, σ_{12}) caused by the mismatch of the local stiffness properties in the bonded adjacent platelets. Platelets (made of unidirectional prepreg tape) in different layers have different extensional stiffness in the global ($x_1x_2x_3$) coordinate system due to their fiber orientation. In-plane stress gradients produce the out-of-plane, or "interlaminar", stresses (σ_{33}, σ_{13}, σ_{23}) in the overlaps between platelets. The details of the three-dimensional stress transfer between platelets in a PPMC depend on the characteristics of the composite meso-structure. The in-plane strength properties of the platelet material are typically greater than the out-of-plane strength properties. Therefore, the stress transfer between platelets is deemed more efficient when out-of-plane stresses are reduced, mitigating premature disbonding between platelets and maintaining the integrity of the meso-structure to a greater applied load, thus allowing the platelets to build more in-plane stress and the composite to achieve a greater strength. In the previous work for the PPMC systems with layered morphology and deterministic orientation state [47,45], authors demonstrated that the platelet length-to-thickness ratio (L_p/t_p) and the geometrical arrangement of platelets are the parameters controlling the efficiency of stress transfer between the platelets. The present work demonstrates the relevance of this principle for the stochastic PPMC as well. Specifically, an increased platelet slenderness (length-to-thickness) ratio tends to improve the stress transfer efficiency (reduce delaminations between platelets) and helps increasing the composite effective properties.

The number of platelets in the system (platelet count) is linked to the concepts of internal redundancy and alternative load path [48,49]. Without redundancy, a structural system fails immediately under local damage developed when the most highly stressed region reaches the local strength. By contrast, the redundant structural system finds new load paths, which enable redistribution of load previously carried by

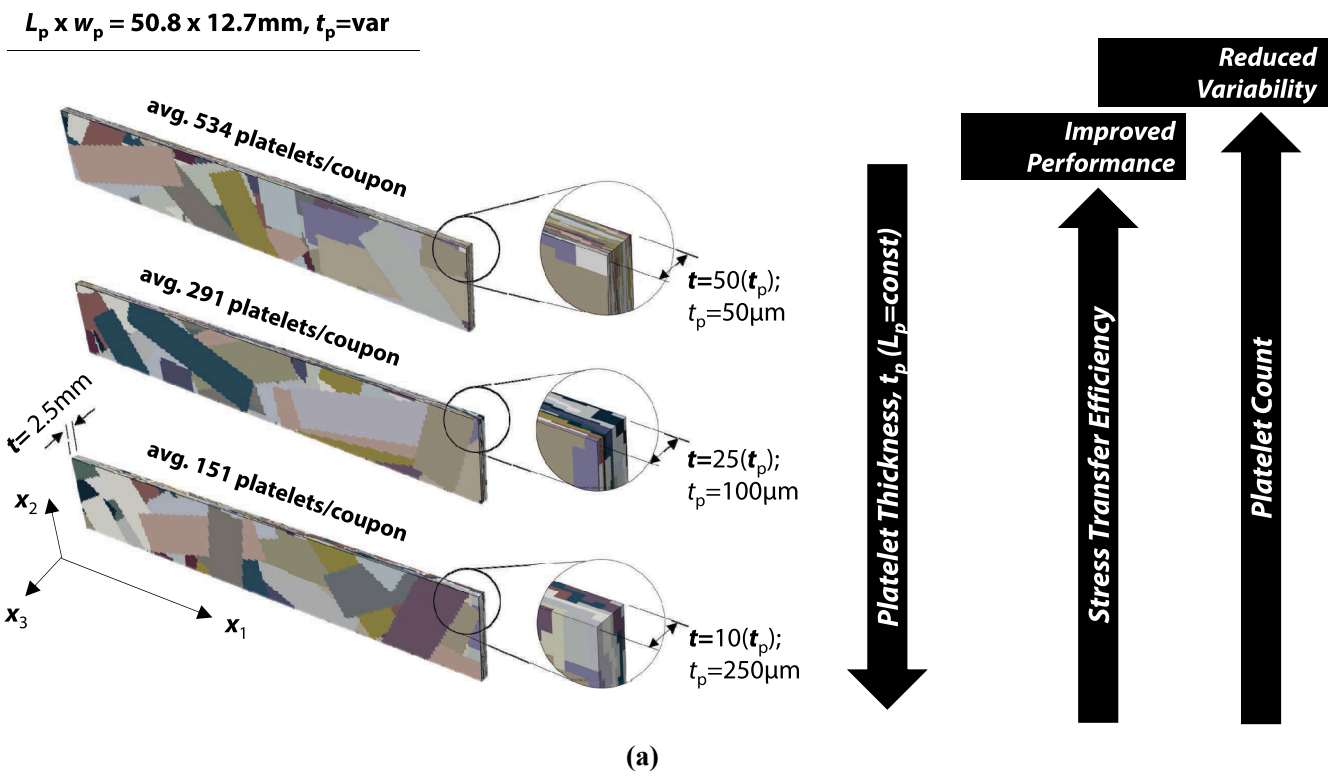

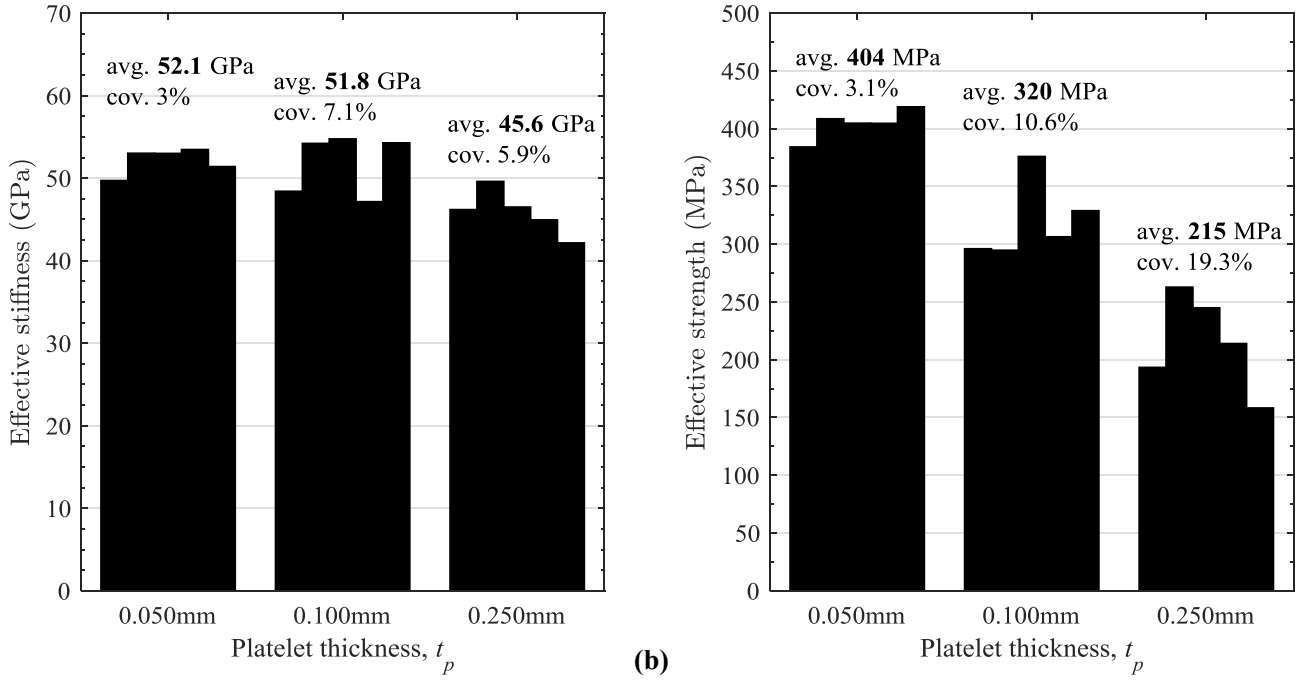

Fig. 17. Simulated effect of platelet thickness on tensile properties of coupons with stochastic morphology. (For interpretation of the references to colour in this figure legend, the reader is referred to the web version of this article.)

now damaged/failed portions. Redundancy can arrest damage propagation and delay the ultimate failure of the system. When a structural system has enough redundancy and there are many alternative load paths, the system failure happens progressively. Increased platelet count leads to the increased internal redundancy of a PPMC system, as more platelets may collectively sustain more widespread damage such that the entire system may hold on to more load before ultimate failure takes place.

Orientation distribution of platelets is an important factor that influences the mechanical performance of a PPMC since orthotropic mechanical properties of a platelet are a function of orientation. Orientation state may depend on different factors. For instance, an increased degree of alignment of a stochastic orientation state can be achieved by the manufacturing process. Next, platelet count may influence a stochastic orientation state in a probabilistic fashion. Since there is a limited number of platelets and orientations within a given volume of a stochastic PPMC, fewer/more platelets imply having fewer/more possible stochastic orientations. With fewer platelets/

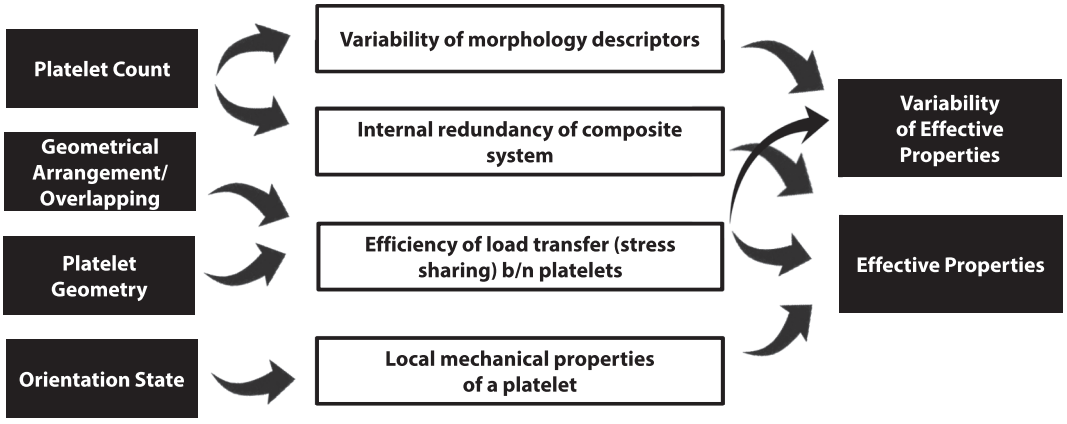

Fig. 18. Implications of PPMC meso-structure descriptors for the performance characteristics.

orientations, one may expect more orientation dissimilarity between composite volumes and more local orientation dissimilarity within a volume, while more platelets/orientations provide for the increased probability of having more uniform orientation state both locally and globally. By the same token, a larger number of platelets mitigates the chances to obtain a local region with a low alignment of platelets with loading direction. Therefore, as a rule-of-thumb, increased platelet count reduces the local variability of meso-scale morphology in a probabilistic sense, i.e. a stochastic PPMC with a greater platelet count would tend to have increased internal redundancy and a smaller scatter in improved mechanical properties.

As a stochastic PPMC is a complex system, the descriptors of the PPMC meso-structure may interact and influence one another, meaning a variation of one meso-structure descriptor may cause changes to some other descriptors. A simple example of such interaction is the above-mentioned influence of platelet count on the stochastic orientation state, while the platelet count itself can be changed by the platelet size. The platelet count can be directly increased by increasing the composite volume $V_2 > V_1$ (e.g. by increasing the tensile coupon thickness), but it can also be modified by the platelet size as there would be a greater count of smaller platelets in the same size volume V_1. Therefore, the platelet size controls the effective properties of a stochastic PPMC by controlling the stress transfer efficiency between the neighboring platelets and by influencing the number of platelets in the composite system, which correlates with the degree of structural redundancy and number of orientations in the composite system.

5. Conclusions

The virtual tensile test series were performed to obtain the distributions of effective stiffness and strength from the digital PPMC coupons with approximate stochastic 3D meso-structure as a function of varying control parameters of the meso-structure. Meso-scale resolution of progressive failure analysis was used to simulate a uniaxial tensile test, for that individual platelets constituting a coupon meso-structure were explicitly modeled as homogeneous orthotropic material with mechanical properties of prepreg tape. The platelet material was assumed to undergo coupled intra- and inter-platelet damage processes, which were mathematically treated by continuum damage mechanics.

Experimental studies showed that improved effective tensile properties in a stochastic PPMC can be achieved by increased composite thickness and enhanced alignment of platelets with loading direction.

The variability of effective tensile properties caused by the variability of stochastic meso-morphology is demonstrated by simulation results. The analysis of statistical significance of the difference between the probabilistic distributions of properties obtained from the virtual and physical test series allowed to validate the simulation framework. The statistical significance methods were also used to compare the property distributions for the modified control parameters of the composite meso-structure.

The virtual testing environment allows to identify how the control parameters of a stochastic PPMC meso-structure determine the effective composite properties and their variability. Such approach aids in understanding the material structure–property relationship and potential property limits. The computational analysis showed that:

(i) the strength of a stochastic PPMC increased with platelet length-to-thickness ratio;
(ii) longer platelets provided for increased variability of effective properties, while the thinner parent tape provided for reduced variability and increased averages of stochastic PPMC effective properties;
(iii) the increased thickness of a stochastic PPMC improves the average tensile stiffness and strength;
(iv) the overall alignment of platelets with the loading direction in a stochastic PPMC improves average tensile stiffness and strength.

The simulated results are in a reasonable agreement with the available experimental measurements of effective tensile properties of a stochastic PPMC.

Declaration of Competing Interest

The authors declared that there is no conflict of interest.

Acknowledgements

The authors wish to thank the Boeing Company for supporting this work (under Master Agreement No. 2011-042). The authors declared that there is no conflict of interest.

Appendix A1. Mesh sensitivity study

The accuracy of the PFA in a virtual coupon in response to the voxel mesh refinement is investigated. The five meshes were considered having voxel in-plane (x_1-x_2) dimensions of 0.1 × 0.1, 0.2 × 0.2, 0.4 × 0.4, 0.7 × 0.7, and 1.0 × 1.0 mm. The voxel thickness was equal to the platelet thickness. First, a virtual coupon discretized with the finest voxels was generated. The coupon in-plane dimensions were as in Section 3.4, the coupon thickness was 2 mm, the platelet dimensions were $L_p \times w_p \times t_p = 12.7 \times 12.7 \times 0.1$ mm and the 2D-random ODF was used. Next, the orientation state was mapped onto the coarser meshes using the nearest neighbor algorithm to produce several FE discretizations of the same meso-scale

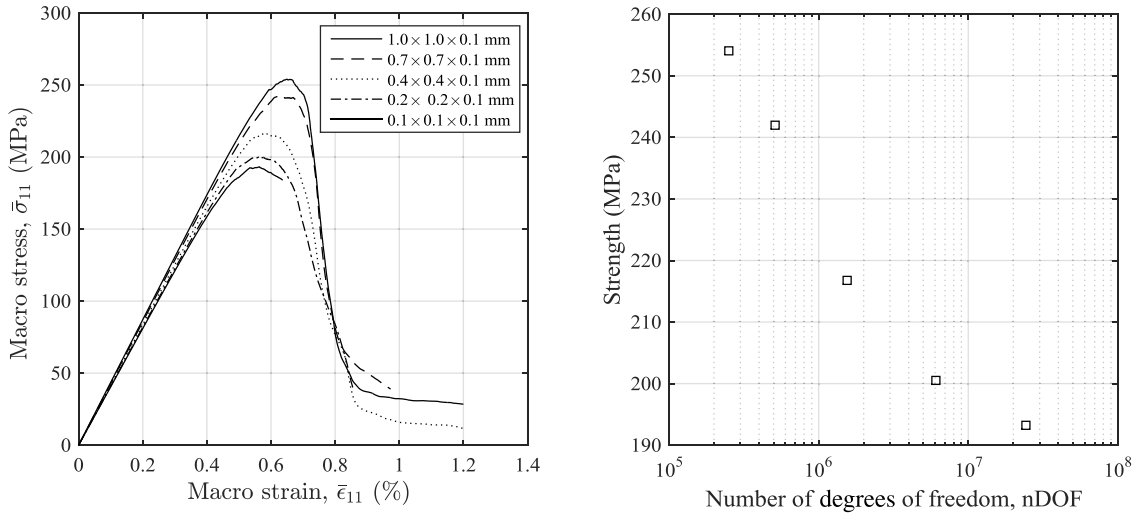

(a)

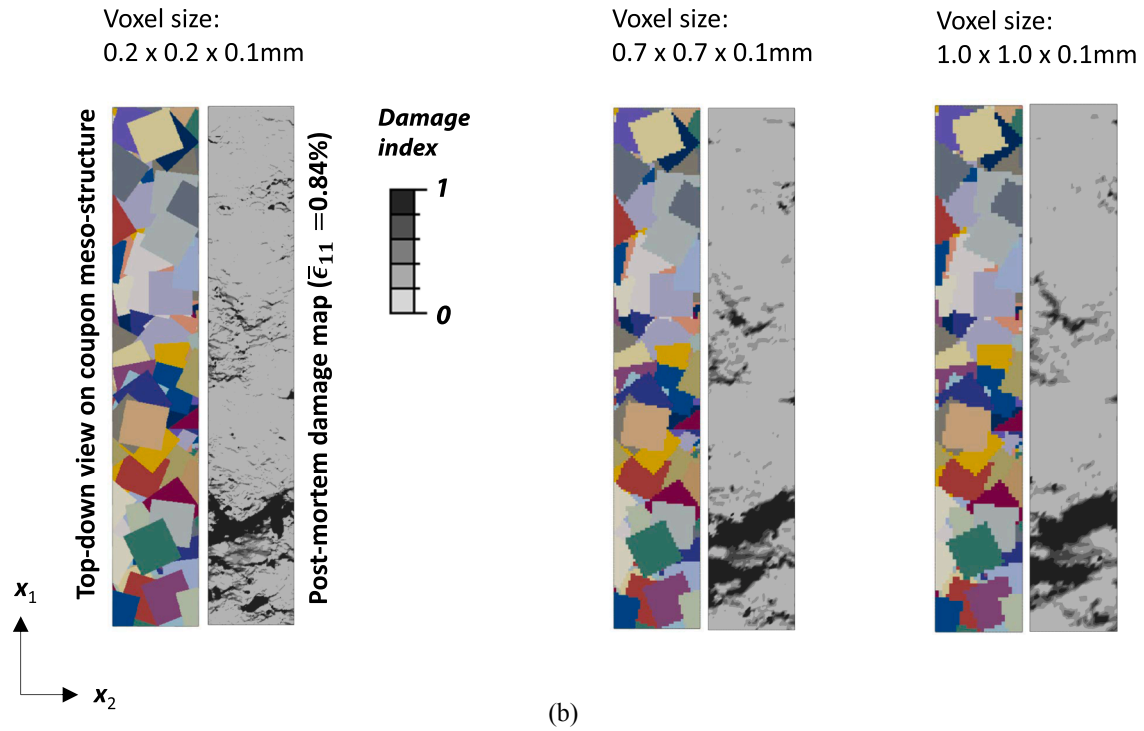

(b)

Fig. A1. Mesh sensitivity study in the PFA of a virtually generated stochastic PPMC coupon: (a) effective stress-strain curves for variable voxel size; (b) view on the coupons for several voxel sizes and corresponding post-mortem damage maps (at $\bar{\epsilon}_{11}$ = 0.84%).

Table A1
Computational time vs mesh refinement in a virtual coupon with a given meso-structure

Voxel size $x_1 \times x_2 \times x_3$ (mm)	No. of degrees of freedom (nDOF)	Load fraction/Applied strain	No. of CPUs	Wall clock time
1.0 × 1.0 × 0.1	250,617	1.0/1.2%	80	2 h 25 m
0.7 × 0.7 × 0.1	508,161	0.811/0.973%	80	4 h 26 m
0.4 × 0.4 × 0.1	1,536,195	1.0/1.2%	80	17 h 56 m
0.2 × 0.2 × 0.1	6,088,764	0.712/0.854%	80	66 h 35 m
0.1 × 0.1 × 0.1	24,227,283	0.552/0.662%	80	241 h 23 m

morphology with different mesh densities. Two factors from mesh refinement are a better platelet shape and a more accurate stress analysis. Fig. A1 (a, on the left) shows the effective stress-strain curves $\bar{\sigma}_{11}(\bar{\epsilon}_{11})$ obtained from the PFAs of all constructed meshes. Decreased in-plane dimensions of a voxel provide for a better aspect ratio of a solid FE allowing a more accurate stress analysis. Smaller elements give an improved resolution of the local stresses, which are primary factors that determine the failure initiation. The effective stiffness decreases and the stresses at local discontinuities increase (which makes the effective strength to decrease) as the element size decreases, both are typical trends in the FEA. When mesh size is

reduced, the energy dissipated through the progressive fracture of a specimen (calculated as area under the stress-strain curve) is also reduced. Fig. A1 shows that the location of the ultimate failure remains nearly the same at different voxel sizes, but the shape of the major failure site naturally is more smeared ("blurry") when mesh is coarsened. The ultimate strength tends to converge at the voxel size of 0.1 × 0.1 × 0.1 mm (24,227,283 degrees of freedom), as Fig. 8 (a, on the right) shows. Increased accuracy of the PFA on a very fine mesh comes at a price of significantly increased computational time even when multiple CPUs are utilized, as Table A1 shows, making such analysis impractical for probabilistic modeling. Therefore, a deliberate choice in favor of a coarser mesh with voxel in-plane dimensions of 0.7 × 0.7 mm is made for the following work, as it compromises an acceptable accuracy and computational cost.

Appendix A2. Effect of Thermal-Residual stress on tensile strength of a stochastic PPMC

A thermos-elastic analysis was developed to determine the thermal-residual stresses in a stochastic PPMC coupon. The model assumes that the stress-free temperature is defined as glass transition temperature (T_g). It is assumed that a virtual specimen is subjected to a uniform temperature differential of $\Delta T = -135\,^{\circ}\mathrm{C}$ for the thermal-residual stress analysis, for $T_g = 160\,^{\circ}\mathrm{C}$ [45] and room temperature is 25 °C. The PPMC coupon is subsequently subjected to progressive failure analysis by applying the mechanical tensile strain. This allows quantification of the thermal-residual stress effect on the ultimate tensile strength of a composite. The coupon and platelet dimensions are as described in Section 3.4. Fig. A2 compares the macroscopic stress-strain curves from a virtual tensile test of the coupon with and without previously applied temperature differential. The progressive failure response of the stochastic PPMC coupon is somewhat affected by the account of the thermal-residual stresses. More macroscopic progressive softening results from the thermal-residual stresses residing in a coupon. Nonetheless, the predicted ultimate strength of a coupon does not seem to be substantially affected by the account of the thermal-residual stresses, being reduced from 224 MPa to 217 MPa (i.e. by 3%). Both analyses showed similar distributions of local damage and identical location of the ultimate failure (macroscopic crack).

Total five stochastically generated coupons (same dimensions and same platelet size) were analyzed for the effect of thermal residual stress on the tensile strength. The strength reduction caused by the thermal-residual stresses was found to be in the range of 3–6%.

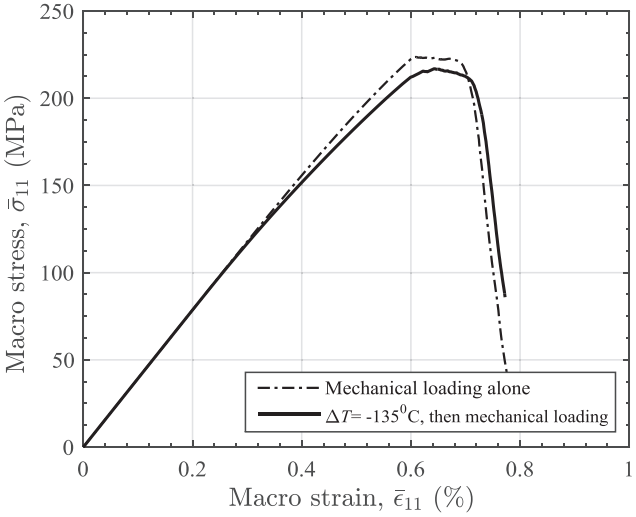

Fig. A2. Effect of thermal-residual stress on the effective tensile response of a stochastic PPMC coupon.

References

[1] Aubry J. HexMC—bridging the gap between prepreg and SMC. Reinf Plast 2001;45(6):38–40.
[2] Fudge JD. Chopped prepregs – compelling performance and cost effective material. SAMPE Conference 41st ITSC, Wichita KS Oct 19-22nd, 2009. 2009.
[3] LeBlanc D, Landry B, Levy A, Hubert P, Roy S, Yousefpour A. Compression moulding of complex parts using randomly-oriented strands thermoplastic composites. SAMPE, Seatle WA. 2014.
[4] Taketa I, Okabe T, Matsutani H, Kitano A. Flowability of unidirectionally arrayed chopped strands in compression molding. Compos B Eng 2011;6(1764–1769):42.
[5] Feraboli P, Peitso E, Deleo F, Cleveland T. Characterization of prepreg-based discontinuous carbon fiber/epoxy systems. J Reinf Plast Comp 2009;28(10):1191–214.
[6] Orgéas L, Dumont PJ. Sheet molding compounds. Wiley Encyclopedia of composites. 2nd ed.Wiley; 2012. p. 2683–718.
[7] Nilakantan G, Olliges R, Su R, Nutt S. Reuse strategies for carbon fiber-epoxy prepreg scrap. CAMX – the composites and advanced materials expo, Orlando, FL, October 13-16. 2014.
[8] Jin BC, Li X, Jain A, González C, LLorca J, Nutt S. Optimization of microstructures and mechanical properties of composite oriented strand board from reused prepreg. Compos Struct 2017;174:389–98.
[9] Lakes R. Materials with structural hierarchy. Nature 1993;361:511–5.
[10] Taketa I, Okabe T, Kitano A. A new compression-molding approach using unidirectionally arrayed chopped strands. Compos A 2008;39:1884–90.
[11] Taketa I, Sato N, Kitano A, Nishikawa M, Okabe T. Enhancement of strength and uniformity in unidirectionally arrayed chopped strands with angled slits. Compos A Appl Sci Manuf 2010;41(11):1639–46.
[12] Visweswaraiah SB, Selezneva M, Lessard L, Hubert P. Mechanical characterisation and modelling of randomly oriented strand architecture and their hybrids–A general review. J Reinf Plast Compos 2018;37(8):548–80.
[13] van Wijngaarden M, Jongbloed A, de Vries J. Thermoplastic compound compression molding. SAMPE, Seatle WA USA. 2010.
[14] Eguemann N, Giger L, Roux M, Dransfeld C, Thiebaud F. Compression moulding of complex parts for the aerospace with discontinuous novel and recycled thermoplastic composite materials. 19th international conference on composite materials. 2013.
[15] Yamashita S, Hashimoto K, Suganuma H, Takahashi J. Experimental characterization of the tensile failure mode of ultra-thin chopped carbon fiber tape-reinforced thermoplastics. J Reinf Plast Compos 2016;35(18):1342–52.
[16] Selezneva M, Lessard L. Characterization of mechanical properties of randomly oriented strand thermoplastic composites. J Compos Mater 2016;50(20):2833–51.
[17] Nicoletto G, Riva E, Stocchi A. Mechanical characterization of advanced random discontinuous carbon/epoxy composites. Mater Today: Proc 2016;3(4):1079–84.
[18] Selezneva M. Experimental and theoretical investigations of mechanical properties of randomly-oriented strand (ROS) composites PhD Thesis McGill University; 2015.
[19] Yamashita S, Sonehara T, Takahashi J, Kawabe K, Murakami T. Effect of thin-ply on damage behaviour of continuous and discontinuous carbon fibre reinforced thermoplastics subjected to simulated lightning strike. Compos A Appl Sci Manuf 2017;95:132–40.
[20] Pech-Canul MI, Kongoli F. The modified central paradigm of materials science and engineering in the extraction and development of new and recycled materials.

Miner Process Extract Metall 2016;125(4):238–41.
[21] Herráez M, González C, Lopes CS, Villoria RGd, LLorca J, Varela T, et al. Computational micromechanics evaluation of the effect of fibre shape on the transverse strength of unidirectional composites: an approach to virtual materials design. Compos A Appl Sci Manuf 2016;91:484–92.
[22] Seneviratne WP, Tomblin J, Jayaratne T. Accelerating composite material qualification using statistically significant multi-scale progressive damage models. CAMX - the composites and advanced materials expo, conference proceedings, Anaheim, CA. 2016.
[23] Feraboli P, Cleveland T, Stickler P, Halpin J. Stochastic laminate analogy for simulating the variability in modulus of discontinuous composite materials. Compos A Appl Sci Manuf 2010;41(4):557–70.
[24] Selezneva M, Roy S, Meldrum S, Lessard L, Yousefpour A. Modelling of mechanical properties of randomly oriented strand thermoplastic composites. J Compos Mater 2017;51(6):831–45.
[25] Li Yizhuo, Pimenta Soraia. Development and assessment of modelling strategies to predict failure in tow-based discontinuous composites. Compos Struct 2019;209:1005–21.
[26] Selezneva M, Roy S, Lessard L, Yousefpour A. Analytical model for prediction of strength and fracture paths characteristic to randomly oriented strand (ROS) composites. Compos B Eng 2016;96:103–11.
[27] Jain A, Jin BC, Nutt S. Mean field homogenization methods for strand composites. Compos B Eng 2017;124:31–9.
[28] Chen Z, Tang H, Shao Y, Sun Q, Zhou G, Li Y, et al. Failure of chopped carbon fiber sheet molding compound (SMC) composites under uniaxial tensile loading: computational prediction and experimental analysis. Compos A Appl Sci Manuf 2018;118:117–30.
[29] Denos BR, Sommer DE, Favaloro AJ, Pipes RB, Avery WB. Fiber orientation measurement from mesoscale CT scans of prepreg platelet molded composites. Compos Part A: Appl Sci Manuf 2018;114:241–9.
[30] Kimoto Y, Murata K, Nuraki T. Thermoplastic composite plate material and products molded from the same. Europe Patent 89312180.6, 23 November; 1989.
[31] Sommer DE. Anisotropic flow and fiber orientation analysis of preimpregnated platelet molding compound PhD Thesis Purdue University; 2018.
[32] Boursier B, Lopez A. Failure initiation and effect of defects instructural discontinuous fiber composites. Hexcel Res Technol 2010.
[33] Snedecor GW, Cochran WG. Statistical methods. Iowa State University Press; 1989.
[34] Forghani A, Shahbazi M, Zobeiry N, Poursartip A, Vaziri R. An overview of continuum damage models used to simulate intralaminar failure mechanisms in advanced composite materials. Numerical modeling of failure in advanced composite materials. Elsevier; 2015.
[35] Digimat User's Manual. Version 2017.0, e-Xstream Engineering. MSC.
[36] Advani SG, Tucker CLI. The use of tensors to describe and predict fiber orientation in short fiber composites. J Rheol 1987;31(8):751–84.
[37] Cintra Jr JS, Tucker CL. Orthotropic closure approximations for flow-induced fiber orientation. J Rheol 1995;6:1095–122.
[38] Groeber MA. Digital representation of materials. Computational methods for microstructure-property relationships. New York: Springer; 2011. p. 99–150.
[39] Abaqus Users Manual. "Version 6.14-1, Dassault Systèmes Simulia Corp.," Providence, RI.
[40] Davila CG, Leone FA. Analysis methods for progressive damage of composite structures. Technical report NASA/TM-2013-218024; 2013.
[41] Linde P, Pleitner J, Boer HD, Carmone C. Modelling and simulation of fibre metal laminates. In ABAQUS Users' conference. 2004.
[42] Bazant Z, Oh B. Crack band theory for fracture of concrete. Mater Struct 1983;16:155–77.
[43] Dávila CG, Camanho PP, Turon A. Effective simulation of delamination in aeronautical structures using shells and cohesive elements. J Aircraft 2008;45(2).
[44] Tay TE, Liu G, Tan VBC, Sun XS, Pham DC. Progressive failure analysis of composites. J Compos Mater 2008;42(18):1921–66.
[45] Kravchenko SG, Sommer DE, Denos BR, Avery WB, Pipes RB. Structure-property relationship for a prepreg platelet molded composite with engineered meso-morphology. Compos Struct 2019;210:430–45.
[46] Saeger KJ, Lagace PA, Shim DJ. Interlaminar stresses due to in-plane gradient stress fields. J Compos Mater 2002;36(2):211–27.
[47] Kravchenko SG, Sommer DE, Pipes RB. Uniaxial strength of a composite array of overlaid and aligned prepreg platelets. Compos A Appl Sci Manuf 2018;109:31–47.
[48] Fang ZX, Fan HT. Redundancy of structural systems in the context of structural safety. Procedia Eng 2011;14:2172–8.
[49] Biondini F, Frangopol DM, Restelli S. On structural robustness, redundancy, and static indeterminacy. Structures congress 2008: crossing borders. 2008.